

CALIFORNIA STATE UNIVERSITY, NORTHRIDGE

THE FRACTIONAL TURN QUADRIFILAR  
HELIX ANTENNA

A thesis submitted in partial satisfaction of the  
requirements for the degree of Master of Science in  
Engineering

by

Charles Eames Seamount

January 1989

© 1988

Charles Eames Seamount

ALL RIGHTS RESERVED

The Thesis of Charles Eames Seamount is approved:

Edmond S. Gillespie (Date)

Leih-Wei Chen (Date)

Sembiam R. Rengarajan, Chair (Date)

# California State University, Northridge

## ACKNOWLEDGEMENTS

The following people not only made this work possible but worthwhile. My loving wife, Martha, whose kind indulgence these three years permitted the completion of this study. My parents, Sidney and Helen, for their support and for instilling in me at an earlier time the competitiveness and will to achieve. Messrs. Don Bowler and Colin Smith for their patience, encouragement and for providing the resources required of this task. Ms. Laraine Simpson for providing the skills necessary to put this work in print. And finally, the Hughes Aircraft Company for creating and maintaining programs such as the MS Microwave Fellowship for its engineers, enabling them to lead the world at the forefront of technology.

## TABLE OF CONTENTS

<u>Title</u>	<u>Page</u>
List of Tables.....	vi
List of Illustrations.....	vii
List of Symbols.....	viii
ABSTRACT.....	xii
CHAPTER 1 Introduction and Background.....	1
CHAPTER 2 Relevant Theory.....	4
2.1 The Geometry of the Fractional Turn Quadrifilar Helix Antenna..	4
2.2 The Derivation of the Moment Method Matrix Equations.....	8
CHAPTER 3 The Moment Method Program.....	22
3.1 Introduction.....	22
3.2 Moment Method Code Description....	22
CHAPTER 4 The Moment Method Solutions.....	25
4.1 Introduction.....	25
4.2 Antenna Input Impedances.....	25
4.3 Antenna Impedance Bandwidths.....	29

## TABLE OF CONTENTS

<u>Title</u>	<u>Page</u>
CHAPTER 5 Further Calculations Utilizing the Moment Method Solution.....	31
5.1 Derivation of the Far Field Electric Field Intensity.....	31
5.2 Comparison of the Radiated Fields.	32
5.3 Polarization Characteristics of the Radiated Fields.....	38
CHAPTER 6 Summary.....	41
6.1 Introduction.....	41
6.2 Results.....	41
6.3 Recommendations for Further Study.	42
REFERENCES.....	44
APPENDIX A Calculated Current Distribution of the Quadrifilar Helix.....	45
APPENDIX B Moment Method Model Input Impedance Data.....	54
APPENDIX C Moment Method Model One-Quarter and One-Half Turn Quadrifilar Helix Radiation Patterns.....	61
APPENDIX D Polarization Characteristics of the Quadrifilar Helix Radiated Field....	78
APPENDIX E Intermediate Moment Method Code Check via the Loop Antenna.....	82

## LIST OF TABLES

<u>Table</u>	<u>Page</u>
1.1      Quadrifilar Helix Parameters of Kilgus.....	3
4.1      Modeled vs. Kilgus Quadrifilar Radiation Resistance and Bandwidth.....	30

## LIST OF ILLUSTRATIONS

<u>Figure</u>		<u>Page</u>
2.1	The Geometry of the Quadrifilar Helix.....	5
2.2	The Generalized Triangle Function $\Lambda_n$ and It's Derivative.....	14
2.3	The Scalar Potential Subdomains.....	17
2.4	The Magnetic Vector Potential Subdomains...	19
4.1	One-Quarter Turn Antenna Input Impedance...	26
4.2	One-Half Turn Antenna Input Impedance.....	27
4.3	One-Turn Antenna Input Impedance.....	28
5.1	One-Quarter Turn Antenna Beamwidth.....	34
5.2	One-Half Turn Antenna Beamwidth.....	35
5.3	One-Quarter Turn Antenna Front-to-Back Ratio	36
5.4	One-Half Turn Antenna Front-to-Back Ratio..	37
5.5	One-Quarter Turn Antenna Axial Ratio.....	39
5.6	One-Half Turn Antenna Axial Ratio.....	40

## LIST OF SYMBOLS

$\vec{A}, \vec{A}(\ell)$	=	the magnetic vector potential
$a$	=	the helix antenna wire radius
$\Delta\ell$	=	the axial length of the helix antenna equal to two pi times the helix pitch times the helix number of turns
$\alpha$	=	the helix pitch angle
$\alpha_a$	=	the auxillary angle defined by the components of the far field electric field
$b$	=	the helix pitch
$c$	=	the helix circumference = $2\pi\rho_0$
$j$	=	$\sqrt{-1}$
$\Delta\ell$	=	the incremental arc length along the antenna wire
$\delta_\theta, \delta_\phi, \delta$	=	the phase of the $\theta$ and $\phi$ electric intensity field components
$\Delta\phi$	=	the incremental angle phi
$\Delta\rho$	=	the incremental radius $\rho$
$\Lambda_m(\ell)$	=	the triangle function
$\vec{E}$	=	the electric intensity field vector
$\ell\Delta\ell$	=	the helix element length
$E_\phi$	=	the $\phi$ directed electric field intensity

LIST OF SYMBOLS (continued)

$E_\theta$	=	the $\theta$ directed electric field intensity
$\epsilon$	=	the permittivity of the medium
$G(\vec{r}, \vec{r}')$	=	the reduced kernel
$I_n$	=	the current at point n
$\vec{J}(\ell)$	=	the current density
$k$	=	the helix element index 0, 1, 2, 3
$\kappa$	=	$2\pi/\text{wavelength}$
$\ell$	=	arc length
$\lambda$	=	wavelength
$m$	=	the observation point index
$\mu$	=	the permeability of the medium
$n$	=	the source point index
NT	=	the helix number of turns
$\eta$	=	the impedance of the medium = $\sqrt{\mu/\epsilon}$
$p$	=	the helix pitch distance = $2\pi b$
$p_\ell$	=	the linear polarization ratio
$\Pi_n(\ell)$	=	the pulse function
$\phi$	=	the angle phi
$\phi_{NP}$	=	the helix terminus angle equal to two pi times the helix number of turns
$\Phi(\ell), \Phi(\vec{r})$	=	the electric scalar potential

LIST OF SYMBOLS (continued)

$\rho_o$	=	the radius of the helix
$\rho$	=	the variable rho along the radial
$\vec{r}_{wk}, \vec{r}_{Hk}$	=	the position vectors of the radial and helix elements
$\vec{r}_o$	=	the far field observation point position vector
$s$	=	$\sqrt{p_o^2 + b^2}$
$\sigma(\ell)$	=	the charge density
$\hat{t}_{wk}, \hat{t}_{Hk}, \hat{t}$	=	the unit tangent vectors along the wire
$\tau$	=	the tilt angle of the polarization ellipse
$V_m$	=	an element of the moment method voltage matrix
$V_o$	=	the source voltage
$\omega$	=	angular frequency in radians per second
$\hat{x}, \hat{y}, \hat{z},$	=	the unit vectors along the x,y,z,
$\hat{r}, \hat{\theta}, \hat{\phi}$	=	$r, \theta, \phi$ directions
$\xi$	=	the ellipticity angle
$Z_{mn}$	=	an element of the moment method impedance matrix

LIST OF SYMBOLS (continued)

$Z_{in}$  = the quadrifilar helix input impedance  
 $z_{k,m,n}, zA_{k,m,n}$  = the subelements of the impedance matrix

ABSTRACT

THE FRACTIONAL TURN QUADRIFILAR  
HELIX ANTENNA

by

Charles Eames Seamount

Master of Science in Engineering

A computer program has been developed which uses the Moment Method to model the fractional turn quadrifilar helix antenna [3]. The currents on the helix antenna wires are determined for helices of one-quarter, one-half and one full turn over a range of frequencies which includes resonance. After computing the currents, various antenna properties are examined. The antenna input impedance, radiation resistance and far field radiation patterns as functions of frequency are generated and compared to earlier researchers' calculated and measured results.

## CHAPTER 1

### INTRODUCTION AND BACKGROUND

The quadrifilar helix antenna has been studied by several researchers. Lumjiak built and characterized several multiturn multifilar helix antennas in 1969 [4]. The antennas characterized were open circuited at the end opposite the feed area. There was also a ground plane associated with each antenna. In 1970 Mendelovicz used numerical methods to derive the far field radiation patterns and scattering properties of multiturn quadrifilar helical antennas [5]. These antennas modeled were of multiturn design similar to Lumjiak's but the effects of a ground plane were not addressed. Adams et al. published a broad overview paper on the quadrifilar helix antenna in 1974 [6]. These researcher's efforts were concentrated primarily on the axial radiation characteristics of the multi-turn quadrifilar helix.

The resonant fractional turn quadrifilar helix antenna, sometimes known as the Kilgus coil, was analyzed by C. C. Kilgus of Johns Hopkins University [1,2,7]. In his 1968 paper Kilgus modeled a one-half turn quadrifilar helix antenna using two orthogonal loop-dipole antennas [2,11]. He assumed a sinusoidal current distribution on

each of the loop-dipoles and the loop-dipole currents were in phase quadrature. The resulting calculated far field radiation pattern was cardioid shaped with the maximum on the helix axis in the backfire direction.

The calculated patterns compared very favorably with the actual measured patterns. The far field radiation pattern was circularly polarized with an axial ratio of close to unity. The circular polarization was obtained when the helix turn area,  $A$ , equalled the helix pitch,  $p$ , times the element length,  $E_l$ . Although not dwelled on, the input impedance of each pair of elements was quoted as being approximately  $50\Omega$ .

The following year Kilgus dismissed the requirement for turn area to equal the pitch times axial length for circular polarization [1]. A circularly polarized cardioid far field radiation pattern was claimed for all axial lengths and diameters except for very large or very small ratios of axial length to diameter and for helical antennas of more than one turn.

In this later model, Kilgus assumed a constant current for the helix radials and a sinusoidal current was assumed for the helical elements. Each opposite pair of wires were fed in antiphase with respect to each other.

And the pairs of wires were in phase quadrature with each other. The antenna patterns were numerically computed with these assumptions. Again, the experimental and computed results agreed very well over the front hemisphere of the antenna. The results were compared for a one-quarter turn, one-half turn and a one-turn quadrifilar helix antenna. Impedance values cited from "limited" data indicated that at resonance, the input impedance of the one-turn helix was approximately 15 ohms. The one-quarter turn antenna impedance was about 70 ohms. Kraus in 1988, although not specific, claimed that the bandwidth for the one-quarter turn quadrifilar helix is approximately 4% [8]. Table 1.1 lists the pertinent parameters of the Kilgus antennas discussed previously. The same parameters are used in the moment method solutions that follow.

Table 1.1. Quadrifilar Helix Parameters of Kilgus  
[1,2,7]

Helix Number of Turns	0.250	0.500	1.000
Resonant Frequency	400 MHz	400 MHz	400 MHz
Wire Diameter	0.00127m	0.001016m	0.00127m
Axial Length	0.2548m	0.2024m	0.1049m
Pitch Angle	67.42°	43.68°	20.37°
Radius	0.06745m	0.06745m	0.04497m
Axial Length/Diameter	1.89	1.50	1.17

## CHAPTER 2

### RELEVANT THEORY

#### 2.1 THE GEOMETRY OF THE FRACTIONAL TURN QUADRIFILAR HELIX ANTENNA

The quadrifilar helix antenna geometry is illustrated in Figure 2.1. The antenna is composed of four elements. Each element is composed of two radials each of length  $\rho_o$  and a portion of a helix of radius,  $\rho_o$ . The helix is a simple curve described by the parameters of pitch,  $b$ , radius,  $\rho_o$ , and the number of turns, NT. Any of the other helix parameters may be determined if these three are known. Each of the elements of the antenna is equally spaced on the circumference of the cylinder defined by the helix radius,  $\rho_o$ . Elements diametrically opposite each other are fed in antiphase. The two diametric pairs are in phase quadrature. The radials of all the elements are all shorted together at the distal end of the helix opposite the antenna feed point. There is no ground plane associated with this antenna.

The moment method solution requires the position vector,  $\vec{r}$ , wire tangent,  $\hat{t}$ , and the wire arc length,  $\ell$ , be known at specified points on the antenna wire.

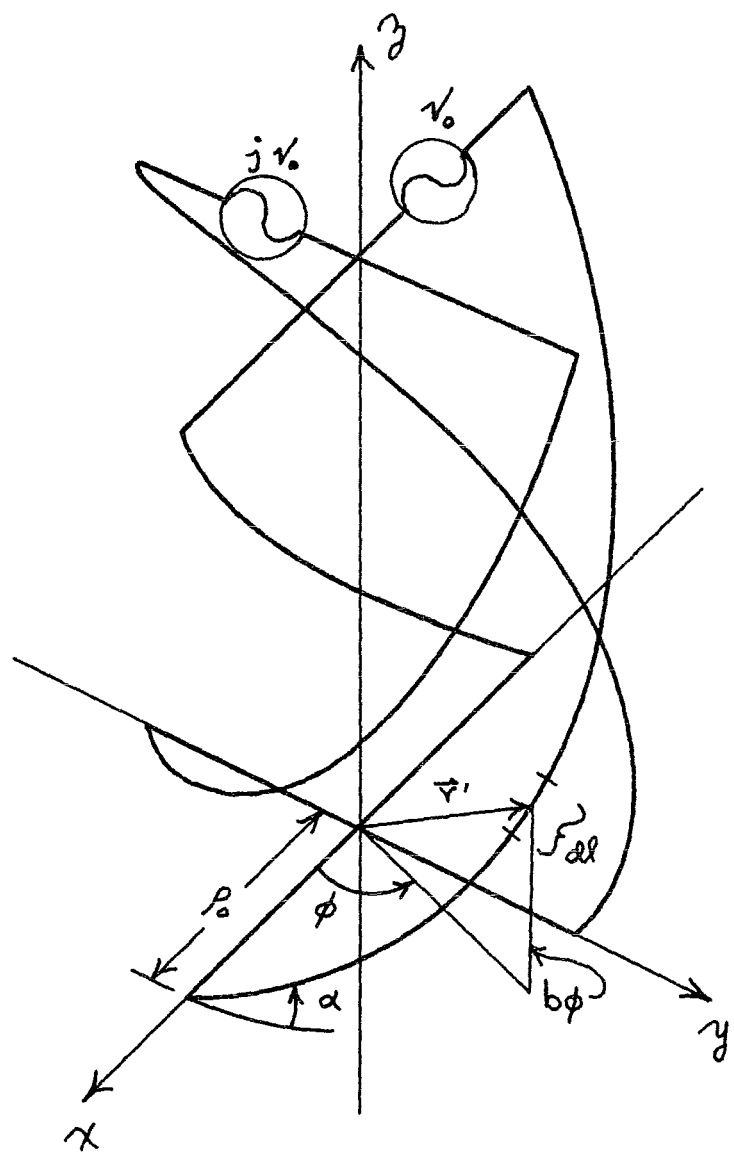


Figure 2.1. The Geometry of the Quadrifilar Helix  
Antenna

For the radial wires at the feed ends, the parameters are

$$\begin{aligned} \vec{r}_{wn,k} = & \rho \cos (\phi_{NP} + k\pi/2) \hat{x} + \rho \sin (\phi_{NP} + k\pi/2) \hat{y} \\ & + b(\phi_{NP} + k\pi/2) \hat{z} \end{aligned}$$

$$n = 1, 2, \dots, N; k = 0, 1, 2, 3$$

The arc length,  $\ell_w = \rho$ , so that

$$\begin{aligned} t_{wn,k}^A = & \frac{\vec{dr}_{wn,k}}{d\ell_w} = \frac{\vec{dr}_{wn,k}}{d\rho} \\ = & \cos (\phi_{NP} + k\pi/2) \hat{x} + \sin (\phi_{NP} + k\pi/2) \hat{y} \end{aligned}$$

At the distal end of the antenna

$$\vec{r}_{wn,k} = \rho \cos (k\pi/2) \hat{x} + \rho \sin (k\pi/2) \hat{y}$$

$$\text{again } \ell_w = \rho$$

$$\text{and } t_{wn,k}^A = \cos (k\pi/2) \hat{x} + \sin (k\pi/2) \hat{y}$$

Each of the helix elements is described by

$$\overset{\rightarrow}{r}_{Hn,k} = \rho_o \cos (\phi + k\pi/2) \overset{\wedge}{x} + \rho_o \sin (\phi + k\pi/2) \overset{\wedge}{y} + b(\phi) \overset{\wedge}{z}$$

The arc length along the helix is

$$l_H = \phi \sqrt{\rho_o^2 + b^2} = \phi s$$

and the tangent at any point then is

$$\overset{\wedge}{t}_{Hn,k} = \frac{\overset{\rightarrow}{dr}_{Hn,k}}{dl_H} = \frac{\overset{\rightarrow}{dr}_{Hn,k}}{sd\phi}$$

$$= \frac{1}{s} \left\{ -\rho_o \sin (\phi + k\pi/2) \overset{\wedge}{x} + \rho_o \cos (\phi + k\pi/2) \overset{\wedge}{y} + bz \right\}$$

## 2.2 THE DERIVATION OF THE MOMENT METHOD MATRIX EQUATIONS

The Method of Moments is used to solve the electric field integral equation (EFIE) at the wire surface [3]. The current distribution on each of the quadrifilar helix elements is determined by enforcing the boundary condition that the tangential electric field is zero at the wire surface.

$$\vec{E}_t^S(\vec{J}, r) = -\vec{E}_t^i(\vec{J}, r) = -[\vec{j}\omega A(r) + \vec{\nabla}\Phi(r)]_t$$

The following thin wire approximations allow one to simplify the EFIE to Pocklington's equation:

- (1) The surface current is circumferentially invariant around the wire.
- (2) The quadrifilar helix element length is much greater than the wire radius, ( $E\ell \gg a$ ).
- (3) The wire radius is much smaller than a wavelength, ( $\lambda \gg a$ ).

Pocklington's equation then can be written

$$-\vec{E}_\ell^i = -j\omega \vec{A}(\ell) - \frac{d\Phi}{dl} \hat{t} \quad \text{on the wire surface}$$

where the vector potential is given by,

$$\vec{A}(\ell) = \frac{\mu}{4\pi} \int_C \vec{I}(\ell') G(\vec{r}, \vec{r}') d\ell'$$

The scalar potential is equal to

$$\Phi(\ell) = \frac{1}{4\pi\epsilon} \int_C \sigma(\ell') G(\vec{r}, \vec{r}') d\ell'$$

into which one can substitute the equation of continuity of current

$$\sigma(\ell) = \frac{j}{\omega} \frac{d\vec{I}(\ell)}{dl}$$

and arrive at the Pocklington equation for a thin wire,

$$\vec{E}_\ell^i = \frac{j\omega\mu}{4\pi} \int_c \vec{I}(\ell) \vec{G}(\vec{r}, \vec{r}') d\ell' + \frac{j}{4\pi\omega\epsilon} \frac{d}{d\ell} \int_c \frac{d\vec{I}(\ell)}{d\ell'} \vec{G}(\vec{r}, \vec{r}') d\ell'$$

This equation can be rewritten by noting that

$$\kappa = \omega\sqrt{\mu\epsilon} \quad \text{and} \quad \eta = \sqrt{\mu/\epsilon}$$

hence,

$$\vec{E}_\ell^i = \frac{j\eta}{4\pi\kappa} \left\{ \kappa^2 \int_c \vec{I}(\ell) \vec{G}(\vec{r}, \vec{r}') d\ell' + \frac{d}{d\ell} \int_c \frac{d\vec{I}(\ell)}{d\ell'} \vec{G}(\vec{r}, \vec{r}') d\ell' \right\}$$

where  $\vec{G}(\vec{r}, \vec{r}')$  represents the reduced kernel

$$\vec{G}(\vec{r}, \vec{r}') = \frac{e^{-j\kappa(|\vec{r}-\vec{r}'|)}}{|\vec{r}-\vec{r}'|}$$

and

$$|\vec{r} - \vec{r}'| = \sqrt{(\vec{r} - \vec{r}')^2 + a^2}$$

$\vec{r}$  = the position vector to the field point

$\vec{r}'$  = the position vector on the wire, source  
point

a = the helix element wire radius.

The primed quantities, ', in all cases indicate source points and the unprimed coordinates are the field observation points.

For the Moment Method solution of weighted residuals, the pulse basis function,  $\Pi_n(\ell)$ , was chosen to approximate the wire currents and the triangle function,  $\Lambda_m(\ell)$ , was chosen as the weighting function.

The pulse basis function is

$$\Pi_n(\ell) = \begin{cases} 1 & , \quad \ell \in (\ell_{n-1/2}, \ell_{n+1/2}) \\ 0 & , \quad \text{elsewhere} \end{cases}$$

and the triangle weighting function is

$$A_m(\ell) = \begin{cases} \frac{\ell - \ell_{m-1}}{\Delta\ell_{m-1/2}}, & \ell \in (\ell_{m-1}, \ell_m) \\ \frac{\ell_{m+1} - \ell}{\Delta\ell_{m+1/2}}, & \ell \in (\ell_m, \ell_{m+1}) \\ 0, & \text{elsewhere} \end{cases}$$

where  $\Delta\ell_{m-1/2} = \ell_m - \ell_{m-1}$  and  $\Delta\ell_{m+1/2} = \ell_{m+1} - \ell_m$ . On the radials, the arc length is

$$\ell_w = \rho \quad \text{and} \quad \Delta\ell_w = \Delta\rho$$

while on the helix the arc length is given by

$$\ell_H = \phi \sqrt{\rho_o^2 + b^2} = \phi s$$

and

$$\Delta\ell_H = \sqrt{\rho_o^2 + b^2} \Delta\phi = s\Delta\phi$$

Substituting the pulse basis function into Pocklington's equation and performing the inner product with the triangle function, one sees immediately that there is a problem with taking the second derivative of the pulse function in the second term. With the use of

reciprocity, the triangle function can be substituted for the currents in the second term so that

$$I(\ell) \underset{\sim}{=} \sum_{n=1}^N I_n A_n(\ell)$$

and

$$\frac{dI(\ell)}{d\ell} \underset{\sim}{=} \sum_{n=1}^N I_n \left[ \frac{\Pi_{n-1/2}(\ell)}{\Delta\ell_{n-1/2}} - \frac{\Pi_{n+1/2}(\ell)}{\Delta\ell_{n+1/2}} \right]$$

See Figure 2.2.

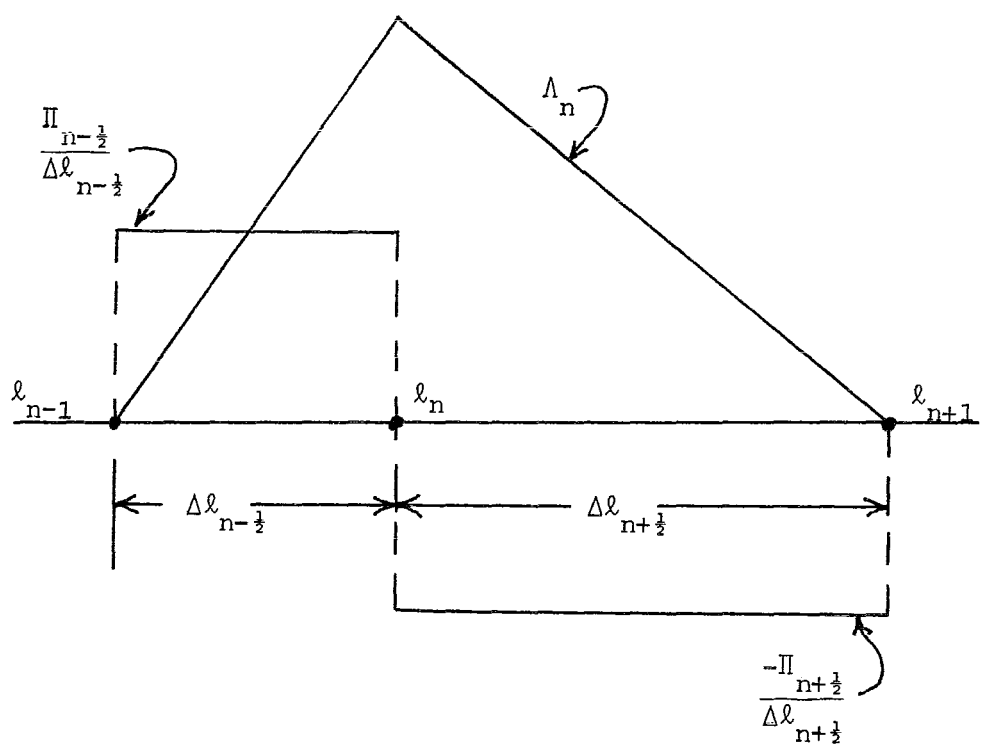


Figure 2.2. The Generalized Triangle Function  $\Lambda_n$  and Its Derivative

The subscripts  $n+1/2$  and  $n-1/2$  indicate that the pulse functions are centered halfway between integer points,  $n$ , on the wire contour or

$$\Pi_{n+1/2}(\ell) = \begin{cases} 1 & , \quad \ell \in (\ell_n, \ell_{n+1}) \\ 0 & , \quad \text{elsewhere} \end{cases}$$

The pulse function is now used as the weighting function for the second term of the equation. Taking the inner product one obtains

$$\langle z_{k,n}, \Pi_m \rangle \approx \sum_{n=1}^N I_n \left\{ \left[ \frac{z_{k,m+1/2,n-1/2} - z_{k,m-1/2,n-1/2}}{\Delta \ell_{n-1/2}} \right] - \left[ \frac{z_{k,m+1/2,n+1/2} - z_{k,m-1/2,n+1/2}}{\Delta \ell_{n+1/2}} \right] \right\}$$

where

$$z_{k,m+1/2,n+1/2} = \int_{\ell_{n+1/2}-\Delta \ell/2}^{\ell_{n+1/2}+\Delta \ell/2} G(\overset{\rightarrow}{r}_{m+1/2}, \overset{\rightarrow}{r}_{n+1/2}) d\ell$$

$$\ell_{n+1/2}-\Delta \ell/2$$

$$z_{k,m+1/2,n-1/2} = \int_{\ell_{n-1/2} - \Delta\ell/2}^{\ell_{n-1/2} + \Delta\ell/2} G(\overset{\rightarrow}{r}_{m+1/2}, \overset{\rightarrow}{r}_{n-1/2}) d\ell$$

$$z_{k,m-1/2,n+1/2} = \int_{\ell_{n+1/2} - \Delta\ell/2}^{\ell_{n+1/2} + \Delta\ell/2} G(\overset{\rightarrow}{r}_{m-1/2}, \overset{\rightarrow}{r}_{n+1/2}) d\ell$$

$$z_{k,m-1/2,n-1/2} = \int_{\ell_{n+1/2} - \Delta\ell/2}^{\ell_{n-1/2} + \Delta\ell/2} G(\overset{\rightarrow}{r}_{m-1/2}, \overset{\rightarrow}{r}_{n-1/2}) d\ell$$

See Figure 2.3.

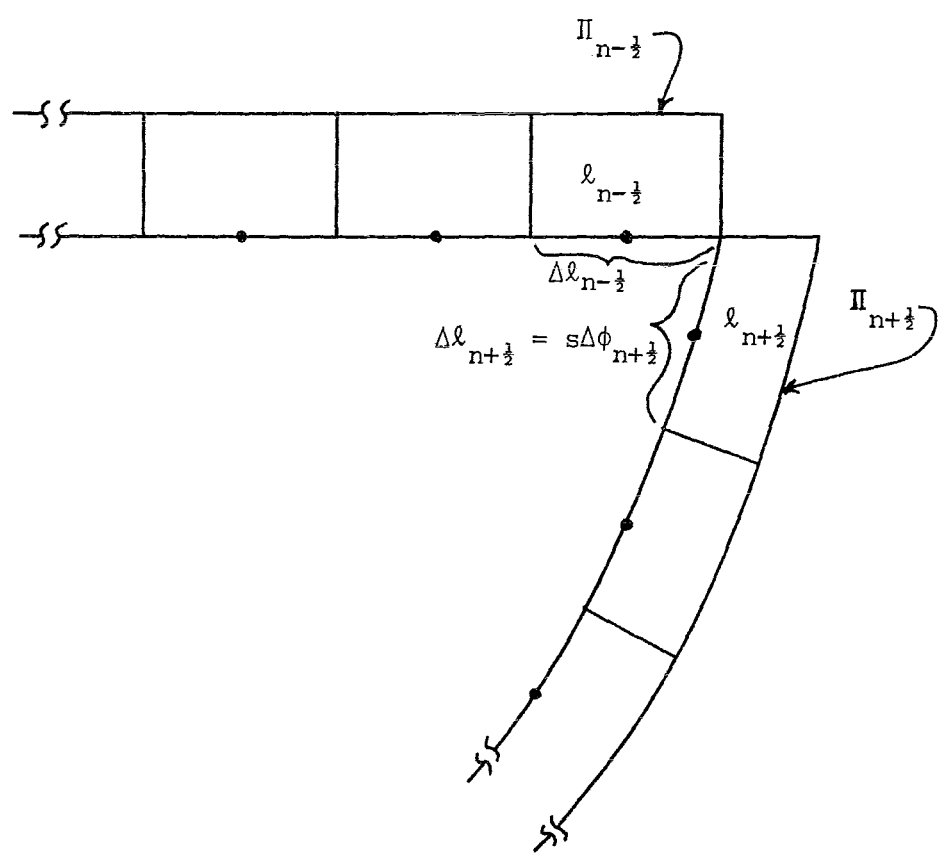


Figure 2.3. The Scalar Potential Subdomains

The first term of the Pocklington equation is not as involved. Using the pulse basis functions, the term

$$\kappa^2 \int_c^\infty \vec{I}(\ell) \vec{G}(r, r') d\ell'$$

can be approximated as

$$zA_{k,n} \approx \kappa^2 \sum_{n=1}^N I_n \int_{\ell_n - \Delta\ell/2}^{\ell_n + \Delta\ell/2} (t \bullet t_n) \vec{G}(r, r_n) d\ell_n$$

Taking the inner product with the triangle function, one arrives at the approximation for the first term of Pocklington's equation. See Figure 2.4.

$$\langle zA_{k,n}, \Lambda_m \rangle \approx \kappa^2 \left[ \frac{\Delta\ell_{m+1/2} + \Delta\ell_{m-1/2}}{2} \right] zA_{k,m,n}$$

Similarly for the  $\delta$ -gap voltage source,  $V_o$ , one performs the inner product of

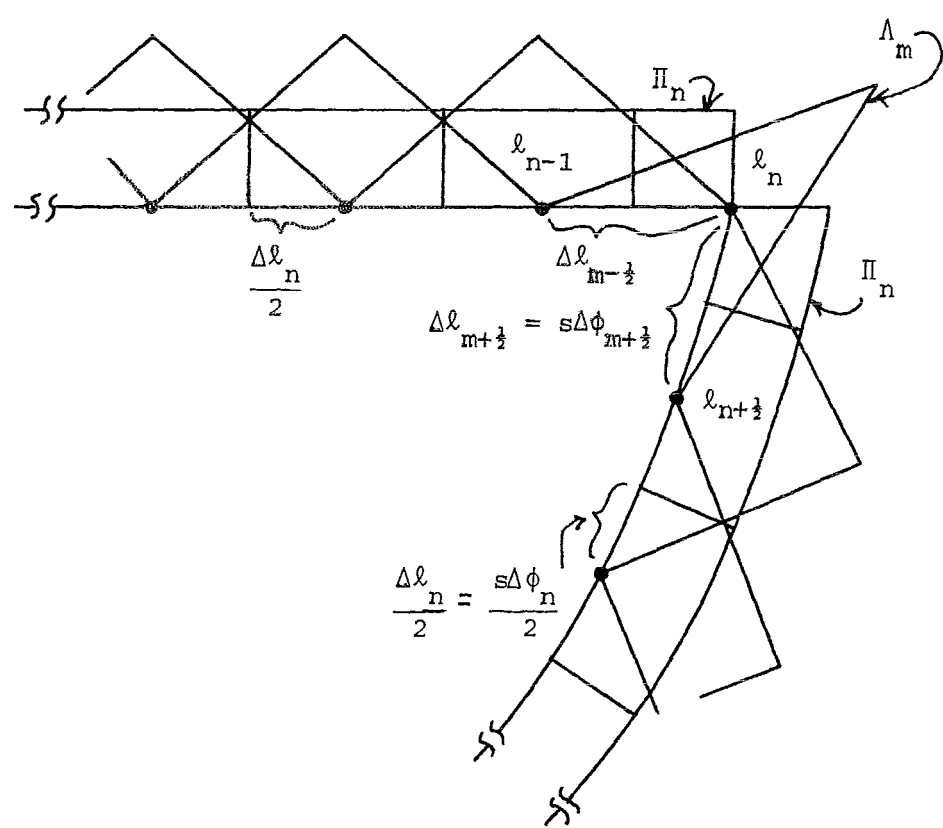


Figure 2.4. The Magnetic Vector Potential Subdomains

$$E_\ell^i \approx \frac{V_o}{\Delta \ell_m} \quad \text{for} \quad 0 \leq \ell \leq \frac{\Delta \ell}{2}$$

and  $\Lambda_m$

so that

$$\langle E_\ell^i, \Lambda_m \rangle \approx \int_0^{\Delta \ell / 2} \Lambda_m E_\ell^i = \frac{V_o}{2}$$

The voltage and impedance matrices can now be formed

$$[V_m] = \begin{bmatrix} -j/2 \\ 0 \\ \bullet \\ \bullet \\ \bullet \\ 0 \\ 0 \\ \bullet \\ \bullet \\ \bullet \\ 0 \\ -j/2 \end{bmatrix}$$

and the impedance matrix can be expressed as

$$[Z_{m,n}]_k = [z_{k,m,n}] + [zA_{k,m,n}]$$

in which a typical element is

$$\begin{aligned} z_{m,n} &\approx \frac{\eta}{4\pi\kappa} \left\{ \begin{bmatrix} -z_{m+1/2,n-1/2} - z_{m-1/2,n-1/2} \\ \Delta\ell_{n-1/2} \end{bmatrix} \right. \\ &\quad \left. - \begin{bmatrix} [z_{m+1/2,n+1/2} - z_{m-1/2,n-1/2}] \\ \Delta\ell_{n+1/2} \end{bmatrix} + zA_{m,n} \right\} \end{aligned}$$

## CHAPTER 3

### THE MOMENT METHOD PROGRAM

#### 3.1 INTRODUCTION

The programs used to generate the currents on each of the antennas and thereby determine the other characteristics were written in FORTRAN on a Digital Equipment Corporation model VAX 8600 computer. The numerical integration routines and the matrix manipulation programs were utilized unmodified from the IMSL Inc. mathematics library of FORTRAN subroutines [10].

#### 3.2 MOMENT METHOD CODE DESCRIPTION

The program requires little interaction with the operator. The inputs required are the subject antenna radius,  $\rho_0$ , in meters, pitch angle,  $\alpha$ , in degrees and the frequency at which the currents are desired in megahertz. All computations are done in wavelengths. The input helix radius is converted to wavelengths and the pitch angle is converted to radians. The next step is to calculate the other requisite parameters,  $\Delta\phi$ ,  $\Delta\rho$ ,  $\Delta\ell$ , etc. The program

then sets about computing all the subelements  $z_{k,m,n}$  and  $zA_{k,m,n}$  as outlined earlier. An IMSL general-purpose integration routine is utilized to perform the integration of the reduced kernel. Once the subelements are all calculated, they are combined to form the elements of the moment method impedance matrix,  $Z_{m,n}$ , as shown previously in Chapter 1. The voltage matrix elements are straight forward. The  $\delta$ -gap voltage source model is employed. The elements at each of the antenna feed points are found equal to  $-j/2$ .

The IMSL mathematic routines are again called. This time to solve the system of complex linear equations

$$[Z_{m,n}]_k [I_{m,n}]_k = [V_m]_k$$

The resultant matrix  $[I_{m,n}]$  is the complex current values at each of the N points of each of the wires of the antenna. The first element of which is also the antenna input admittance. The program goes on to calculate the input impedance of the antenna for the parameters that were given.

A total of 40 match points was chosen for each of the elements. Four were used on each radial and 32 for each of the helix elements for a grand total of 160 points for

each antenna. The choice for the number of points was arbitrary except to keep the subdomain electrical length below 0.37 radians [5].

During the development of the code for the helix, intermediate programs were written. One for the dipole antenna and one for the loop antenna. The results of these helped to confirm that the programming and algorithm was on the right track. The dipole and loop results were as theory would predict. The loop antenna input admittance is given in Appendix E for loop radii of 0.02 to 0.50 wavelengths. The values shown agree extremely well with Harrington's [3].

## CHAPTER 4

### THE MOMENT METHOD SOLUTIONS

#### 4.1 INTRODUCTION

The three quadrifilar helices that were reported on by Kilgus were the subjects of the computer modeling described in Chapters 2 and 3 [1,2]. In Table 1.1 the pertinent characteristics of each of the antennas are listed. The currents for each of the helices were determined over a frequency range of approximately 300 MHz to 850 MHz or axial lengths of about  $0.1\lambda$  to  $0.5\lambda$ .

#### 4.2 ANTENNA INPUT IMPEDANCES

The current distributions derived from the model are plotted in Appendix A as a function of match point for one element of the antenna. The plots are for the one-quarter and one-half turn antennas at the boundaries of the impedance bandwidths, at resonance and at 400 MHz.

The resultant input impedance was then computed as a function of frequency for each antenna. Figures 4.1, 4.2 and 4.3 graphically portray the input impedance as a

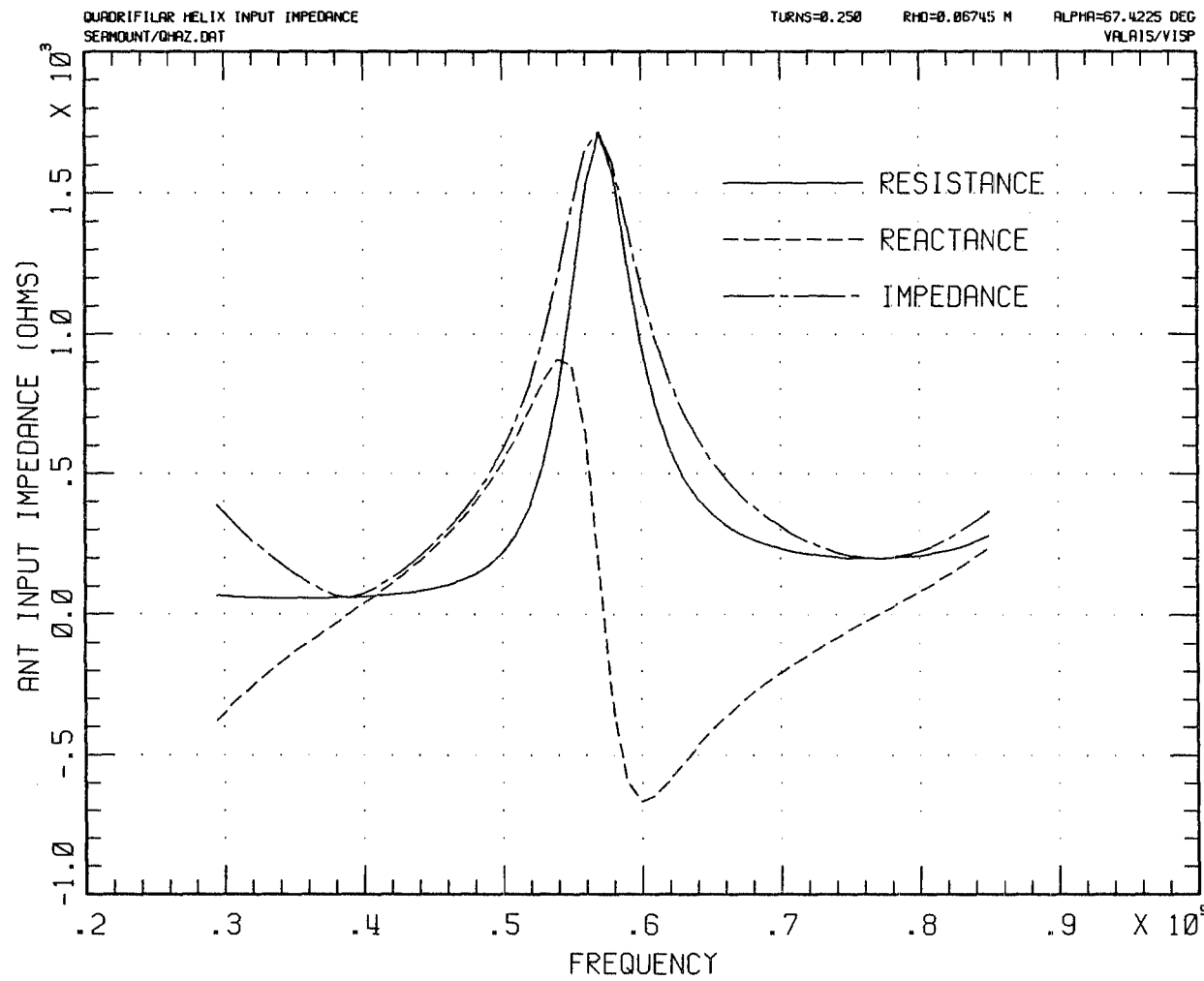


Figure 4.1. One-Quarter Turn Antenna Input Impedance

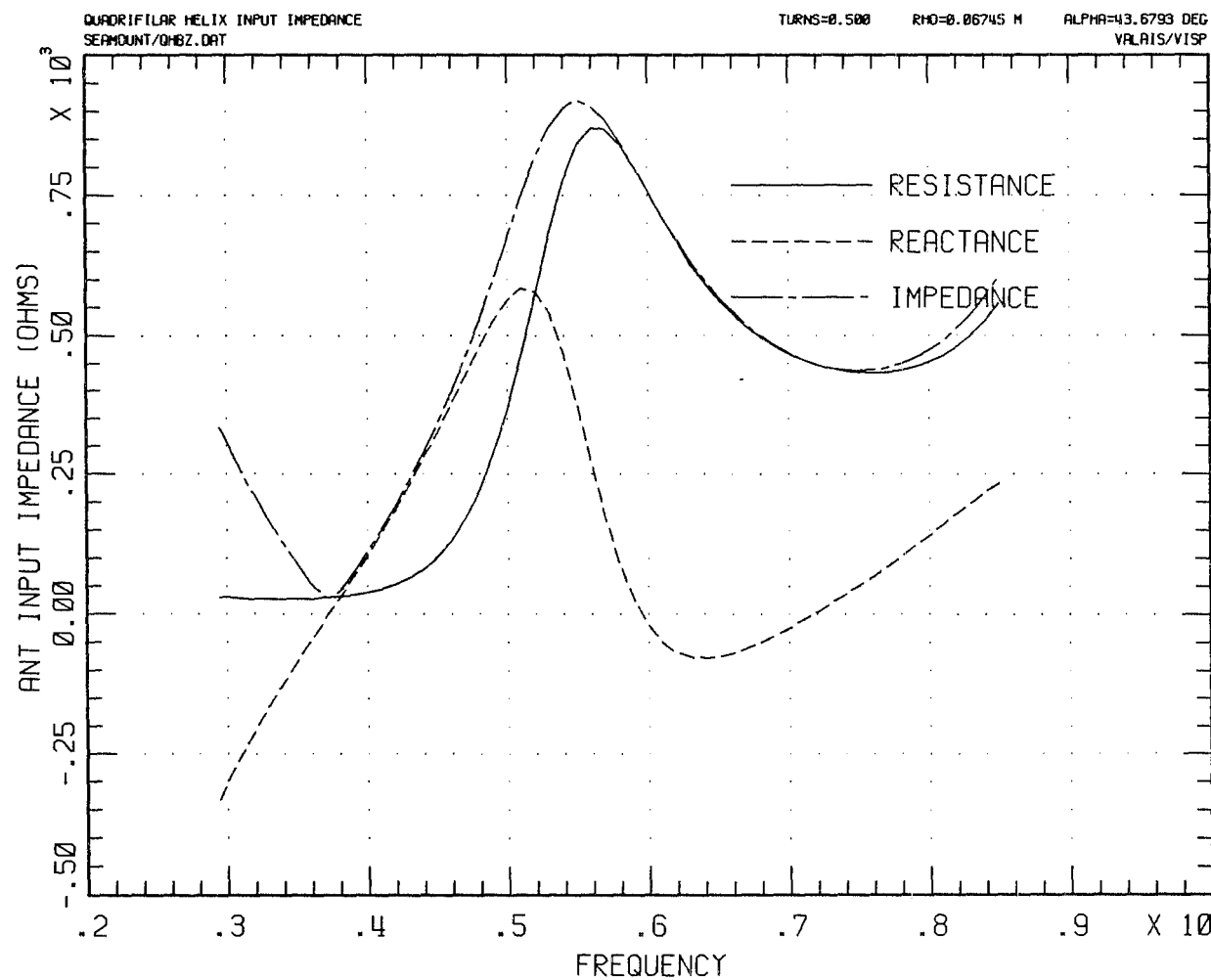


Figure 4.2. One-Half Turn Antenna Input Impedance

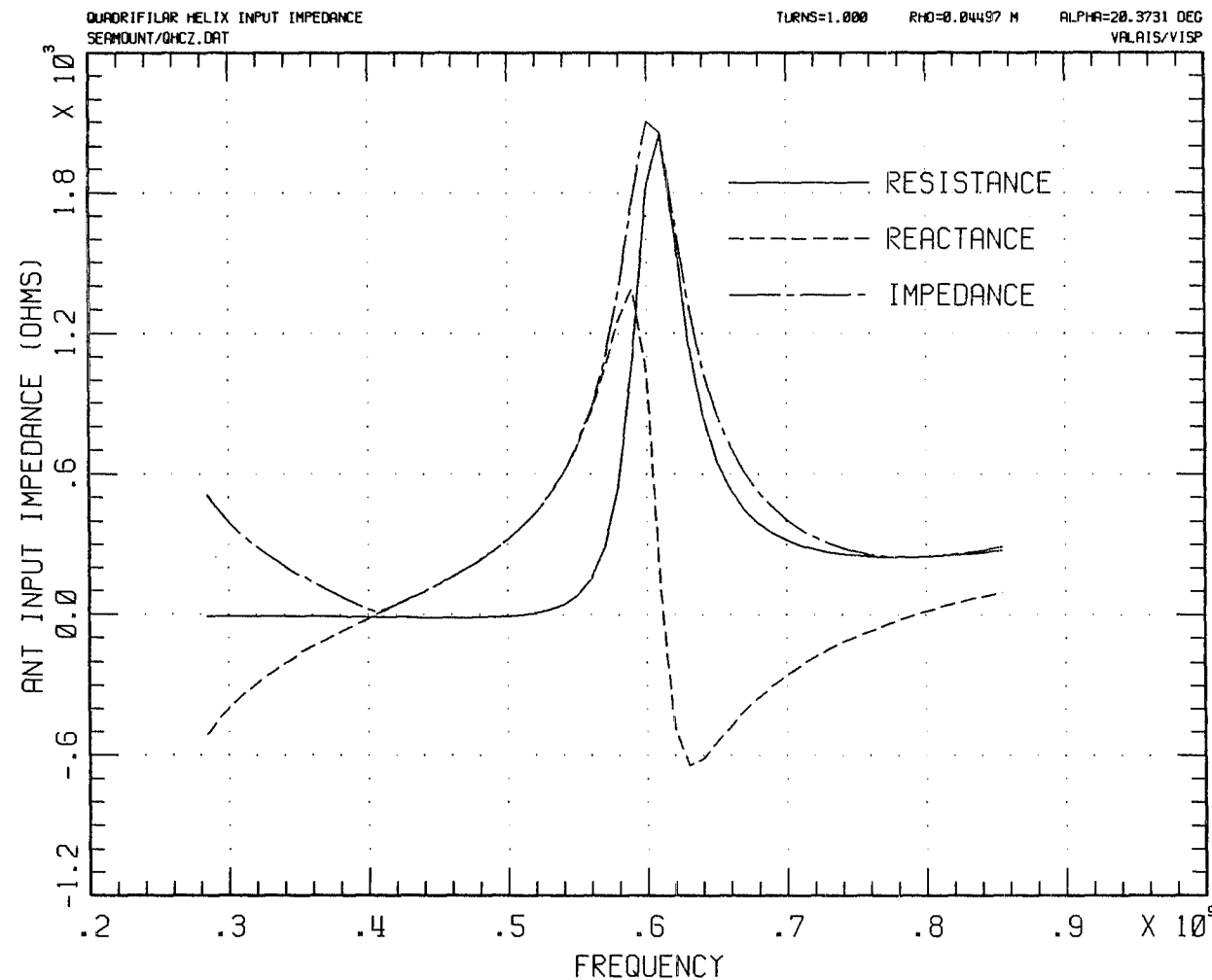


Figure 4.3. One Turn Antenna Input Impedance

function of frequency for the one-quarter turn, one-half turn and one turn quadrifilar helix respectively. The input impedance versus frequency data are tabulated in Appendix B. The resonant frequency of the one-quarter turn helix is seen to be about 390 MHz. The antenna input impedance at this frequency is 60 ohms. The one-half turn helix input impedance at the first resonance is calculated to be 29 ohms at a frequency of 373 MHz. The one turn helix resonant radiating resistance is approximately 12 ohms at about 406 MHz.

Kilgus reported that the magnitude of the input impedance at 400 MHz for the one-quarter turn and one turn antennas as 70 ohms and 15 ohms respectively [1]. His earlier paper states that the radiation impedance of the one-half turn helix is approximately 50 ohms [2]. The data are listed in Table 4.1 for comparison.

#### 4.3 ANTENNA IMPEDANCE BANDWIDTHS

A voltage standing wave ratio, VSWR, of 2:1 was used to determine the impedance bandwidth for each of the modeled antennas. These are also listed in Table 4.1. No

bandwidth data has been quoted by Kilgus. However, Kraus has indicated that the bandwidth of the one-half turn quadrifilar helix is narrow and about 4% [8]. The modeled one-half turn quadrifilar helix bandwidth is seen to be 27 MHz or about 7%.

Table 4.1. Modeled vs. Kilgus [1,2]  
Quadrifilar Radiation Resistance and Bandwidth

	Number Of Turns	Resonant Frequency (MHz)	Bandwidth (MHz)	$ Z_m $ (ohms)
Kilgus [1,2]	1/4	400	---	70
	1/2	400	4%	50
	1	400	---	15
M/M Model	1/4	390	58 (15%)	60
	1/2	373	27 (7%)	29
	1	406	14 (3.5%)	12

## CHAPTER 5

### FURTHER CALCULATIONS UTILIZING THE MOMENT METHOD SOLUTION

#### 5.1 DERIVATION OF THE FAR FIELD ELECTRIC FIELD COMPONENTS

A companion FORTRAN program was also written to determine the far field radiation characteristics of the quadrifilar helix antennas. Once the current distribution generated by the moment method program is known along the wire, the electric far field can be determined. In the far field, the electric field intensity is given by

$$\vec{E} = -j\omega \vec{A}$$

hence, for a filamentary current source by

$$\vec{E} = \frac{-j\kappa\eta}{4\pi r_o} e^{-j\kappa r_o} \int_C I(\ell') e^{j\kappa(\vec{r}_o \cdot \vec{\ell}')} d\ell'$$

Each value of current determined for each wire segment of the moment method solution is treated as an infinitesimal current source.

This allows a summation of each of the contributions in the far field. At the far field observation point, then, the two orthogonal field components can be determined.

$$E_\theta = \frac{-j\kappa\eta}{4\pi r_o} e^{-j\kappa r_o} \left[ \sum_{n=1}^{k*N} I_n \Delta\ell_n (\hat{t}_n \cdot \hat{\theta}) e^{j\kappa(\hat{r}_o \cdot \vec{r}_n)} \right]$$

and

$$E_\phi = \frac{-j\kappa\eta}{4\pi r_o} e^{-j\kappa r_o} \left[ \sum_{n=1}^{k*N} I_n \Delta\ell_n (\hat{t}_n \cdot \hat{\phi}) e^{j\kappa(\hat{r}_o \cdot \vec{r}_n)} \right]$$

The magnitude and phase relationship between these two components allows the characterization of the far field radiation pattern.

## 5.2 COMPARISON OF THE RADIATED FIELDS

Appendix C contains the plotted far field radiation patterns for the one-quarter and one-half turn quadrifilar helix antennas. The patterns are given for the theta, phi and total electric fields. The patterns are cardioid

shaped in the backfire direction near resonance. A small backlobe occurs in the one-half turn antenna which detracts from it's front-to-back ratio. The patterns agree quite well with the data presented by Kilgus for these antennas [1,2]. Figures 5.1 and 5.2 show graphically the 3 dB beamwidths presented by Kilgus and those calculated by the moment method [1,2].

The front-to-back ratios for the two antennas are presented in Figures 5.3 and 5.4. The one-quarter turn helix has a greater front-to-back ratio than that measured by Kilgus with a large peak at resonance. The one-half turn model shows a lower front-to-back ratio. Since the feed and supporting structure are included on the measured antennas, the characteristics of the field will likely be different than the models'.

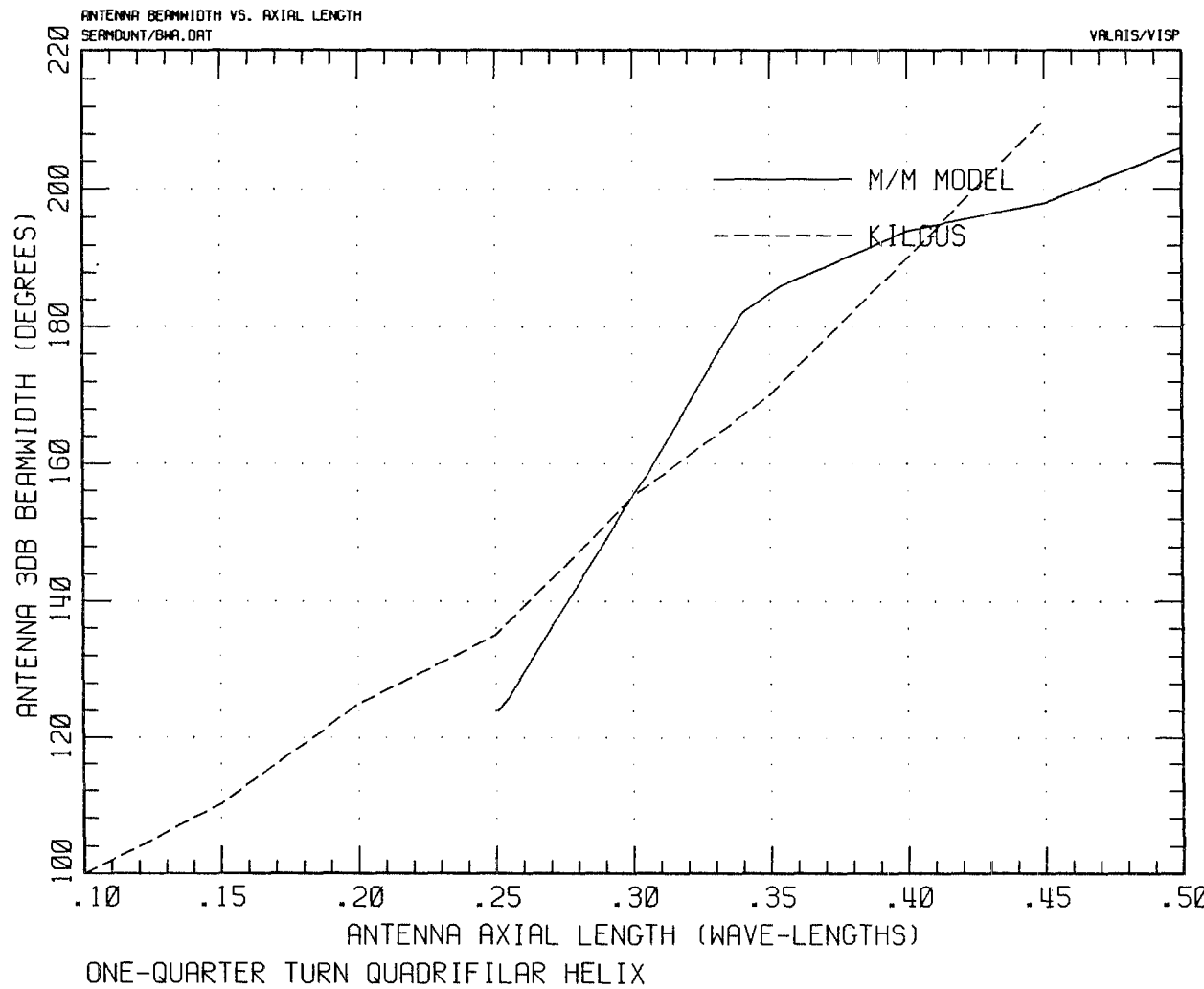


Figure 5-1. One-Quarter Turn Antenna Beamwidth

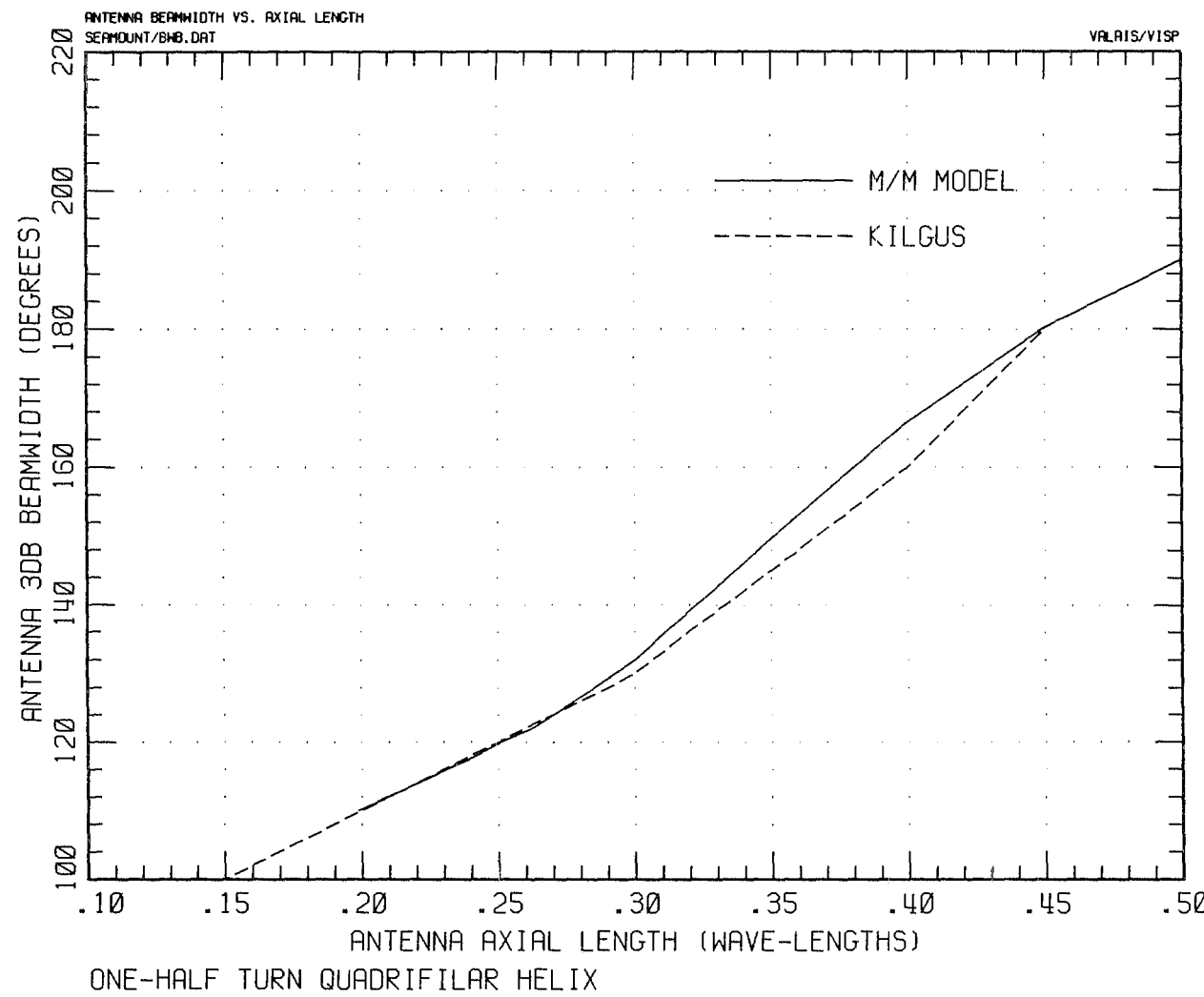


Figure 5.2. One-Half Turn Antenna Beamwidth

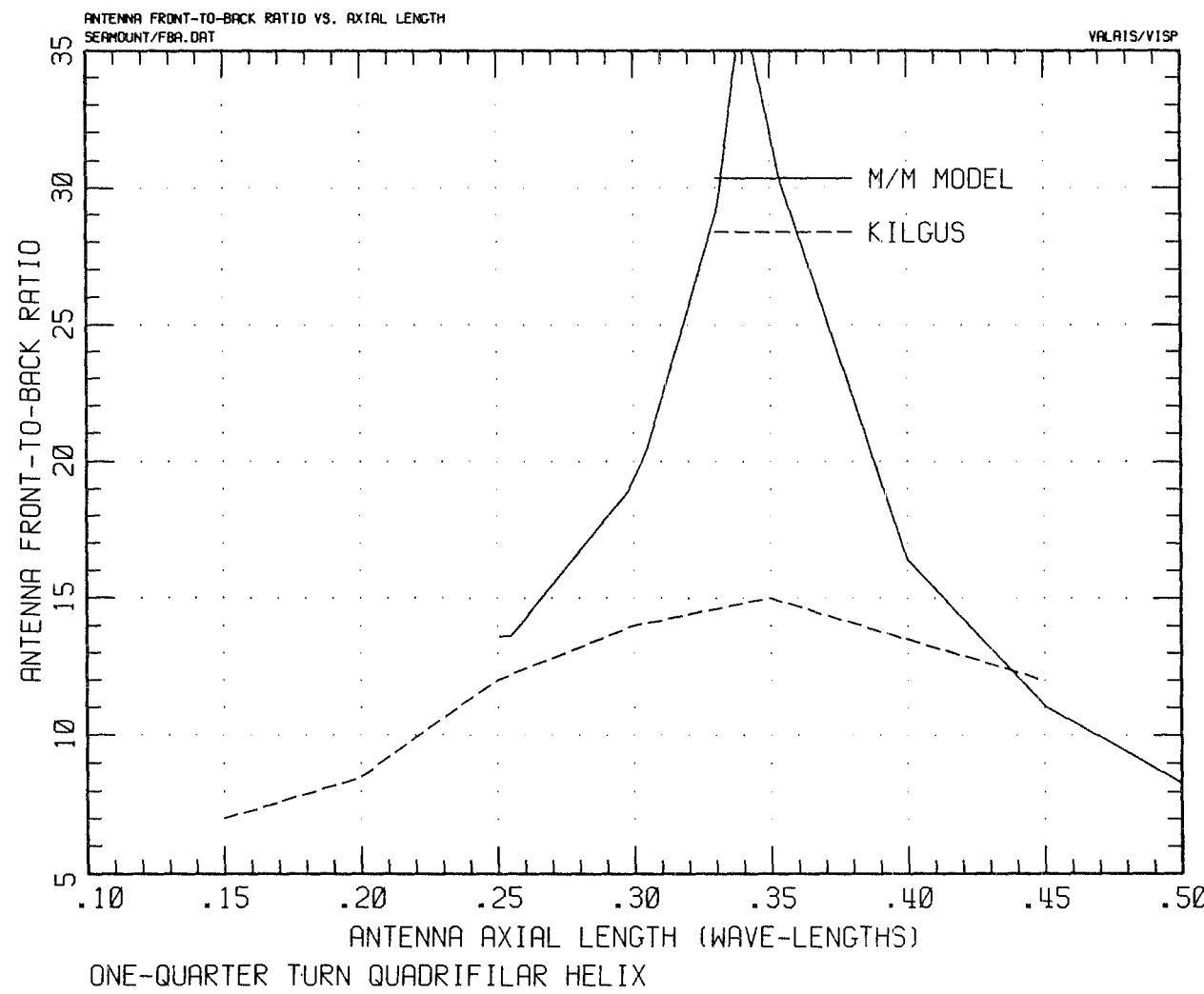


Figure 5.3. One-Quarter Turn Antenna Front-to-Back Ratio

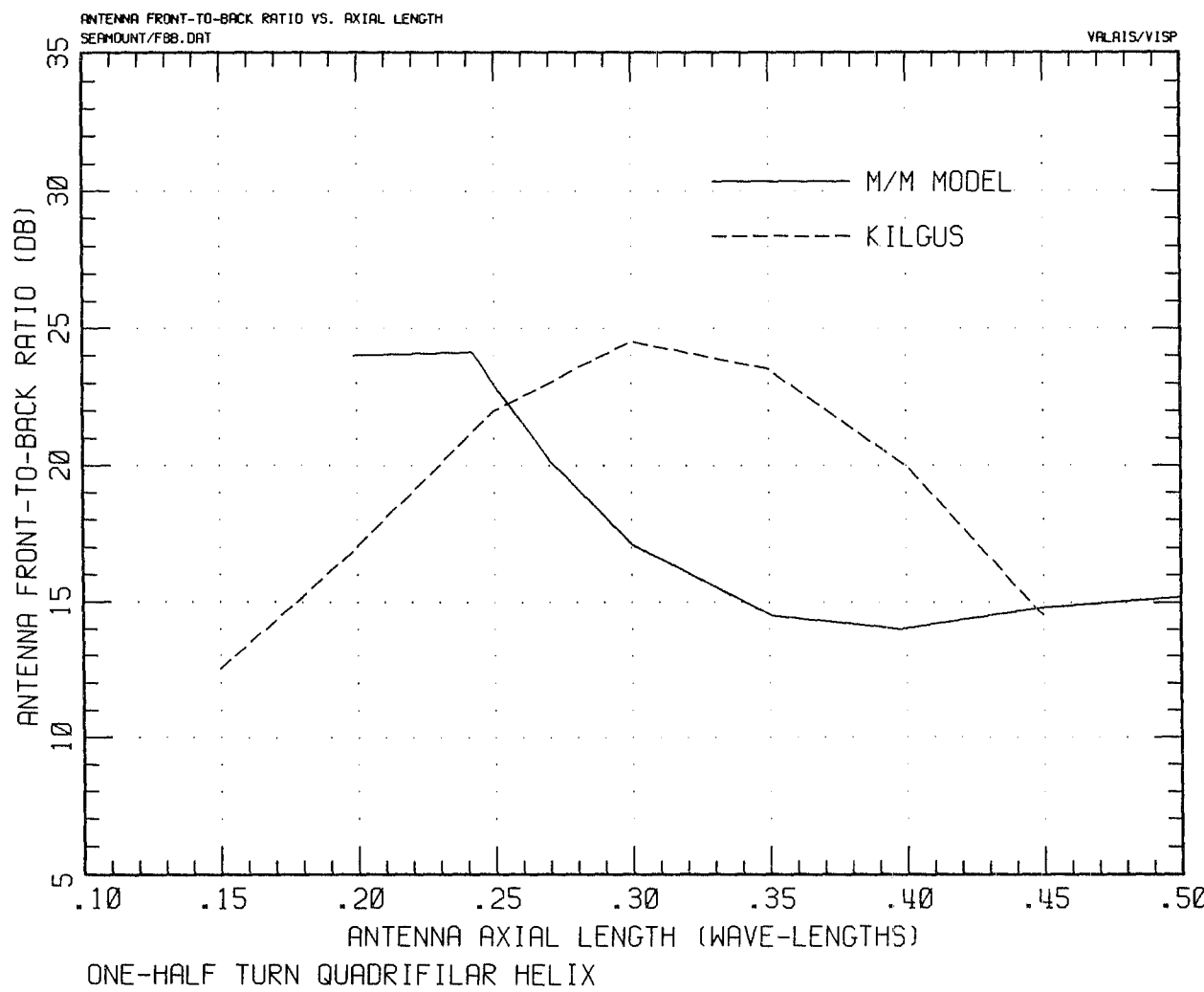


Figure 5.4. One-Half Turn Antenna Front-to-Back Ratio

### 5.3 POLARIZATION

In addition to the magnitude of the far field radiation patterns, the polarization characteristics of the two antennas were calculated. The ellipticity, tilt angle and axial ratio were calculated as outlined in Appendix D. The peak axial ratio over the 3 dB beamwidth and over the front hemisphere are compared with Kilgus' results in Figures 5.5 and 5.6. Although the general shapes of the calculated curves are similar to the empirical data, the calculated results show a slightly higher average axial ratio for the one-quarter turn antenna and slightly lower values for the one-half turn helices. The sign of the calculated axial ratio was used to determine the sense of the polarization. In both cases and at all points, the axial ratio was positive indicating right hand elliptical polarization sense.

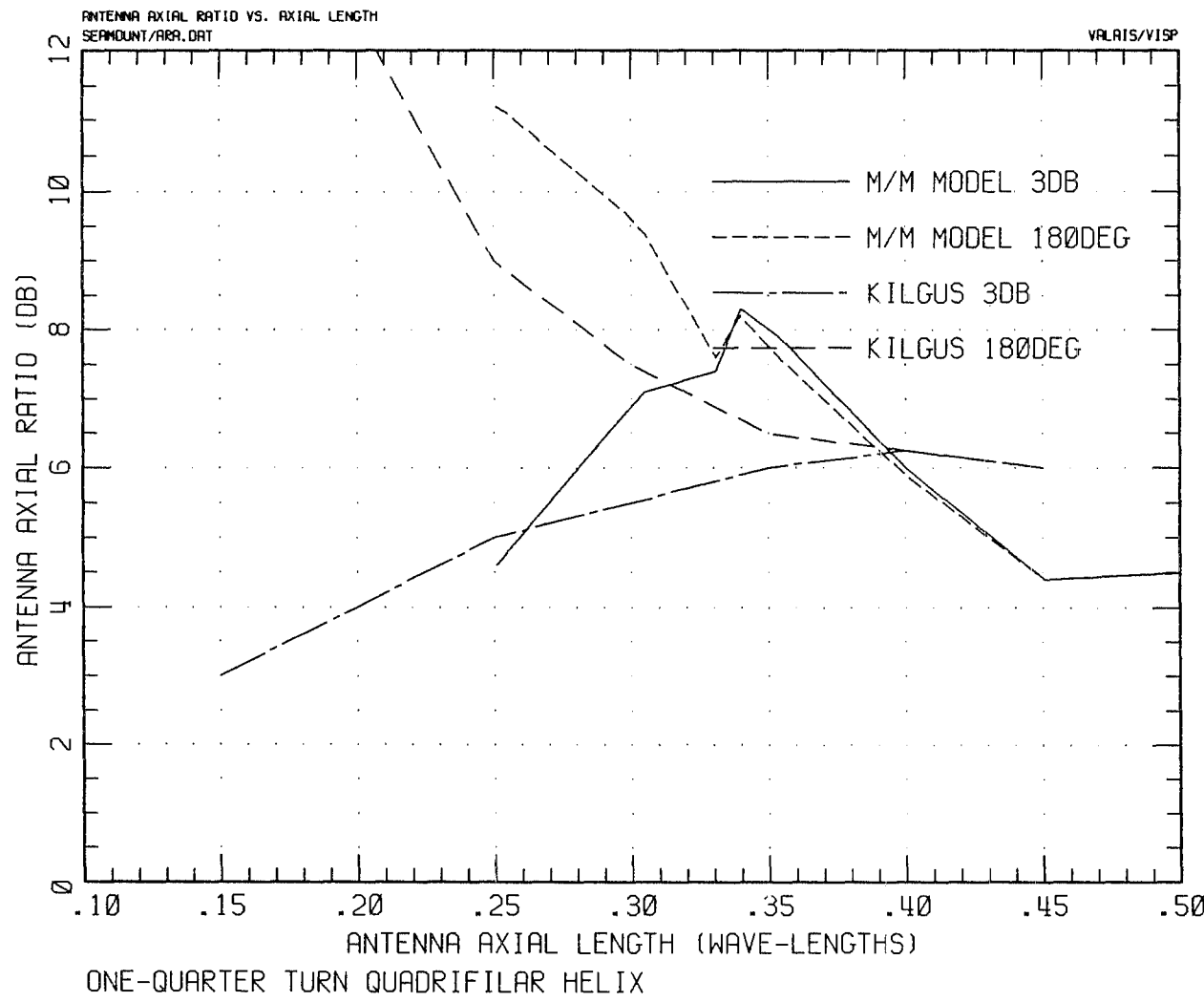


Figure 5.5. One-Quarter Turn Antenna Axial Ratio

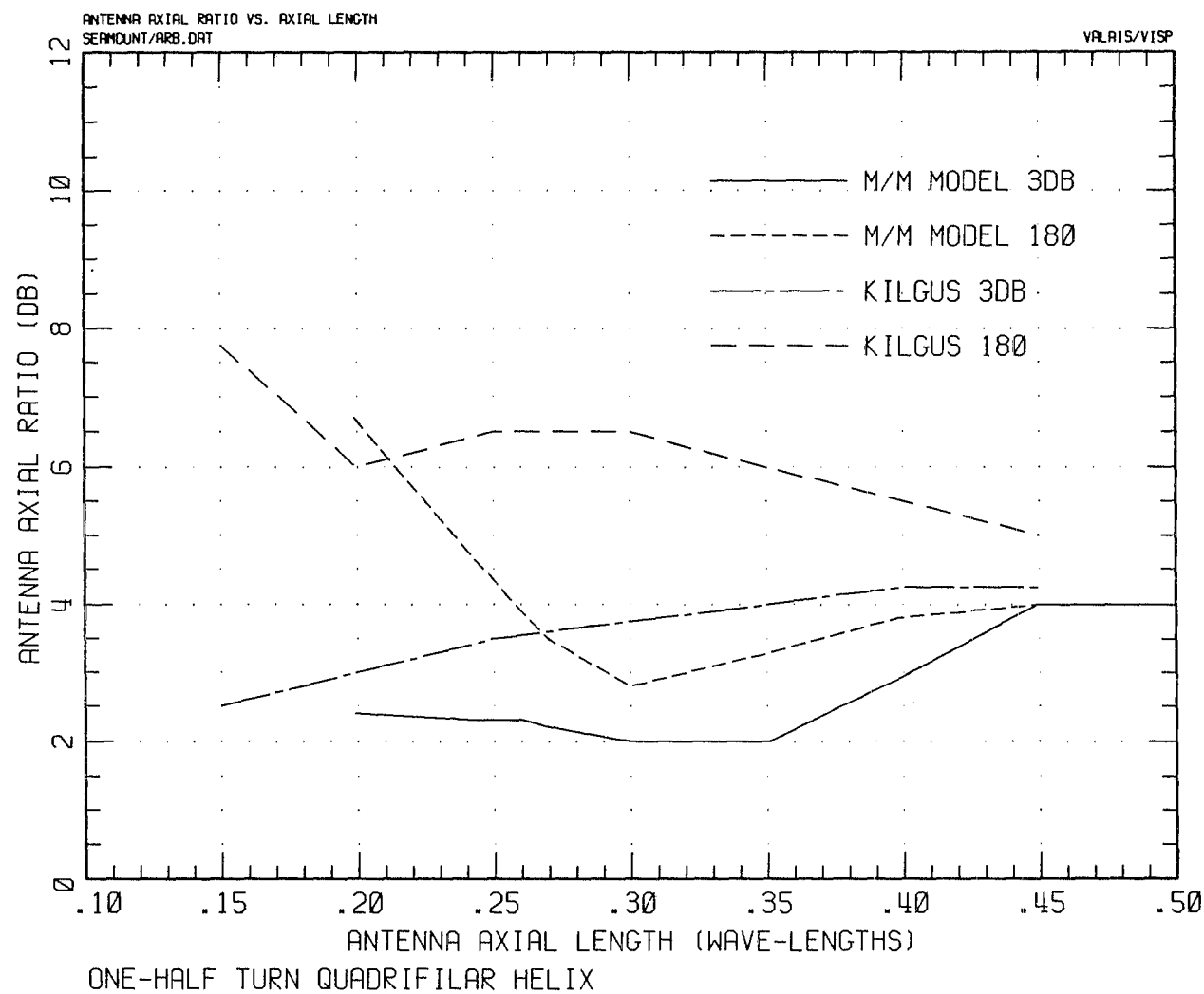


Figure 5.6. One-Half Turn Antenna Axial Ratio

## CHAPTER 6

### SUMMARY

#### 6.1 INTRODUCTION

The method of moments has been used to model the current distribution, over a range of frequencies near resonance, of the fractional turn quadrifilar helix antenna. Numerical techniques were used to determine the antenna input impedance as a function of frequency and the far field radiation patterns. These results were compared with earlier measured and computed data of C. C. Kilgus.

#### 6.2 RESULTS

The resonant input impedances computed and current distributions agreed well with Kilgus' work. The cardioid far field radiation pattern shapes also agreed with the earlier work as did the antennas' 3-dB beamwidths. The peak axial ratios, however, of the modeled antennas exhibited only a passing resemblance in shape to the Kilgus empirical data.

The front-to-back ratio data also did not correlate extremely well with the measured antennas. This could be explained by a slight backlobe on the one-half turn antenna patterns where none exists in the experimental data presented by Kilgus. It should be noted that the Kilgus antennas must have a physically realizable feed network and supporting structure. The modeled antennas assumed an idealized voltage feed and no other structures were included in the model. The variance in the measured data from the modeled antenna characteristics probably is due to these differences. The moment method model seemed to predict quite well, however, the antenna input impedances, pattern shapes and current distribution.

### 6.3 RECOMMENDATIONS FOR FURTHER STUDY

Further investigation of these antennas might include:

- (1) The applicability of the described Moment Method code to antennas of greater than one turn.
- (2) The effects a ground plane might have on the described antenna.

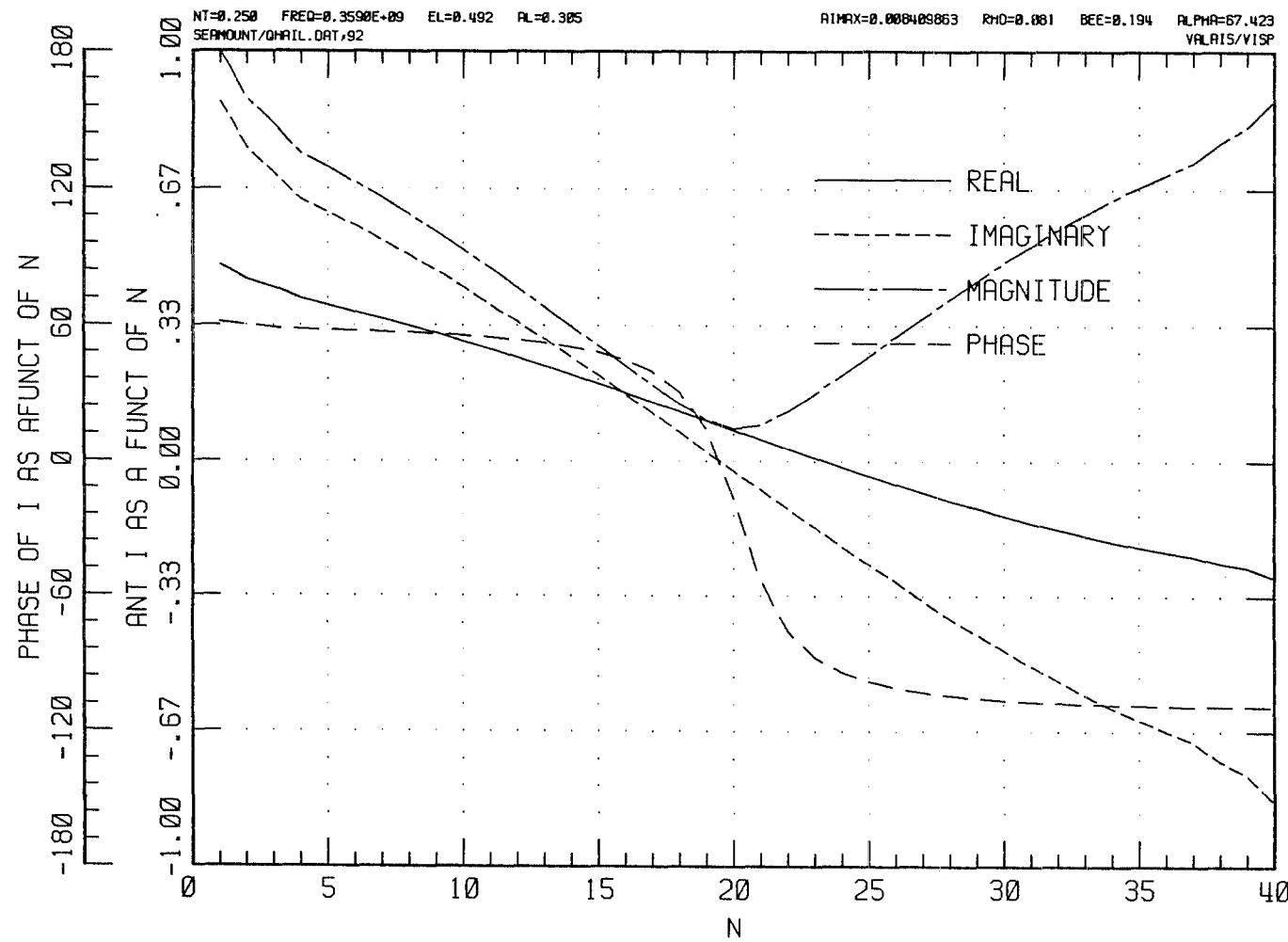
(3) Possibilities of using these antennas as the radiating elements in an array. The broad circularly polarized element pattern may prove interesting in some applications.

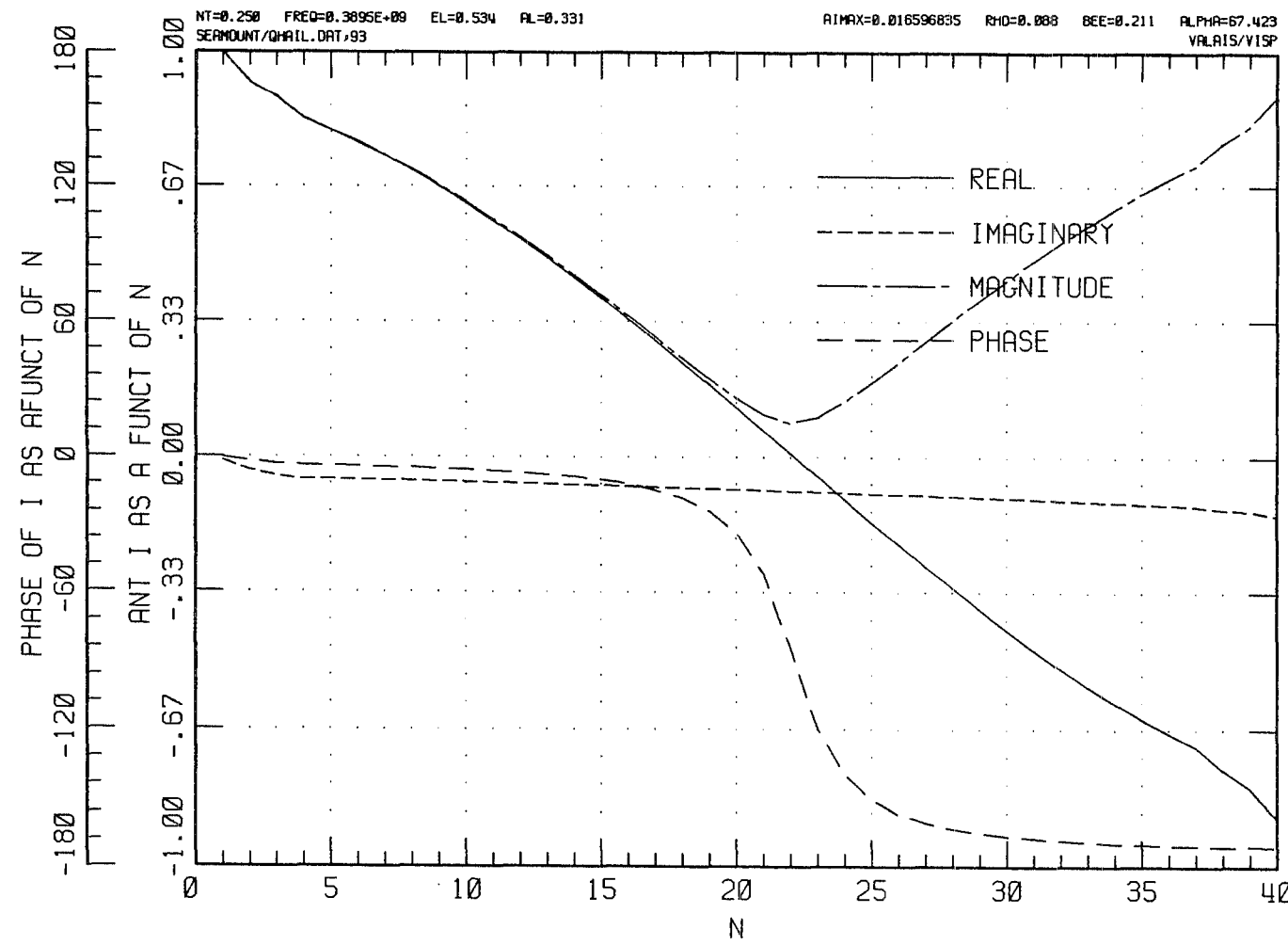
## REFERENCES

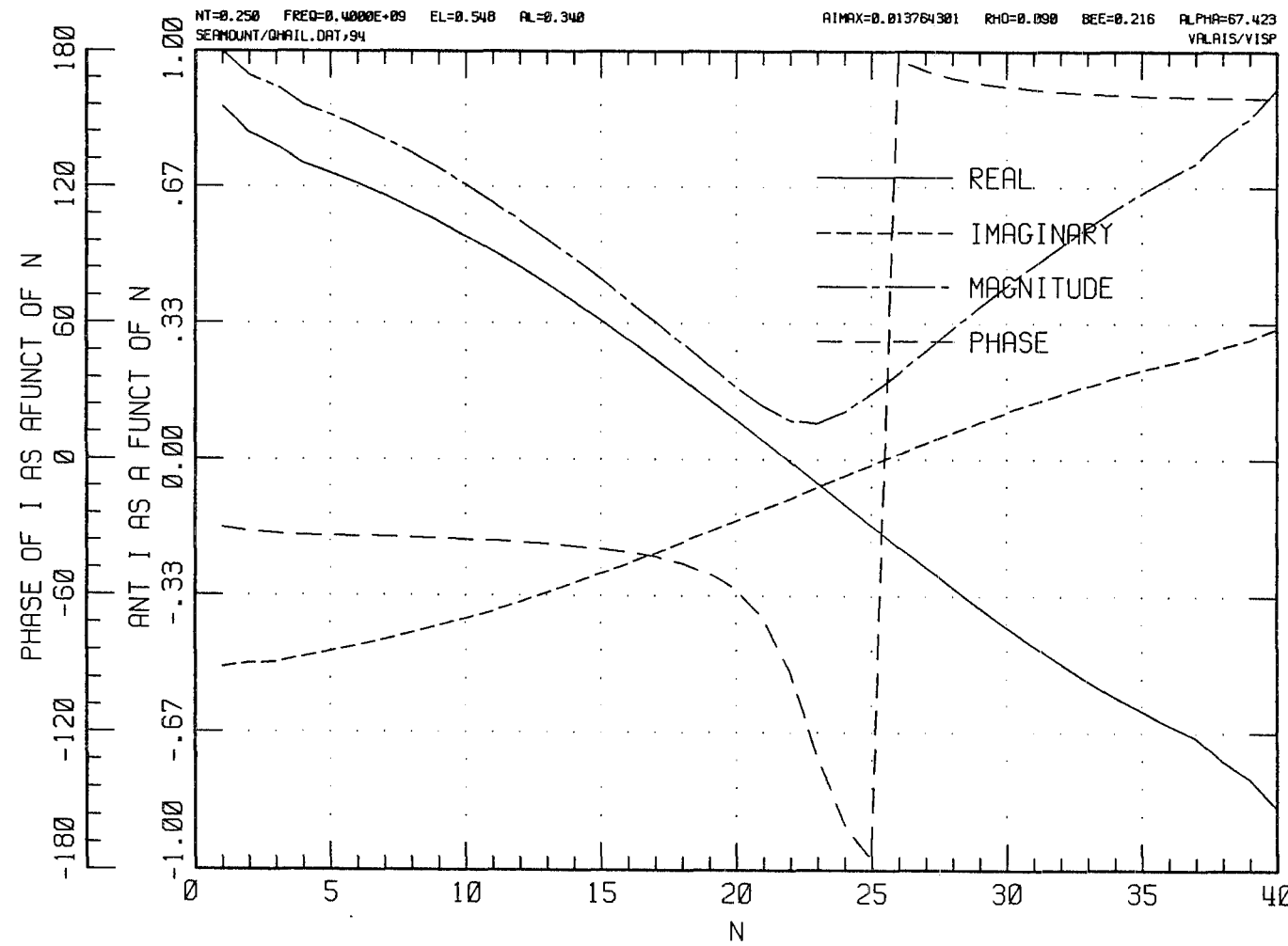
- [1] Kilgus, C. C., "Resonant Quadrafilar Helix," IEEE Transactions on Antennas and Propagation, Vol. AP-17, pp. 349-351, May 1969.
- [2] Kilgus, C. C., "Multielement, Fractional Turn Helices," IEEE Transactions on Antennas and Propagation (Communications), Vol. AP-16, pp. 499-500, July 1968.
- [3] Harrington, R. F., Field Computation by Moment Methods. New York: Macmillan, 1968.
- [4] Lumjak, C., "An Experimental Study of the Quadrifilar Helix Antenna," M.S. Thesis, Department of Electrical Engineering, Syracuse University, Syracuse, New York, November 1969.
- [5] Mendelovicz, A., "Numerical Solution for Scattering and Radiation of a Quadrifilar Helix," M.S. Thesis, Department of Electrical Engineering, Syracuse University, Syracuse, New York, June 1970.
- [6] Adams, A. T., Et. Al., "The Quadrifilar Helix Antenna," IEEE Transactions on Antennas and Propagation, Vol. AP-22, No. 2, pp. 173-178, March 1974.
- [7] Kilgus, C. C., "Shaped-Conical Radiation Pattern Performance of the Backfire Quadrifilar Helix," IEEE Transactions on Antennas and Propagation, Vol. XX, pp. 392-397, May 1975.
- [8] Kraus, J. D., Antennas, 2nd Edition, New York: McGraw-Hill Book Company, 1988.
- [9] Butler, C. M. Et. Al., EE 592/4, Class notes handout, University of Southern California, 1982.
- [10] IMSL, Math/Library User's Manual, Houston, Texas, April 1987.
- [11] Brown, G. H., Et. Al., "Circularly-Polarized Omni-Directional Antenna," RCA Review, Vol. 8, pp. 259-260, June 1947.
- [12] Mott, H., Polarization in Antennas and Radar. New York: John Wiley and Sons, 1986.

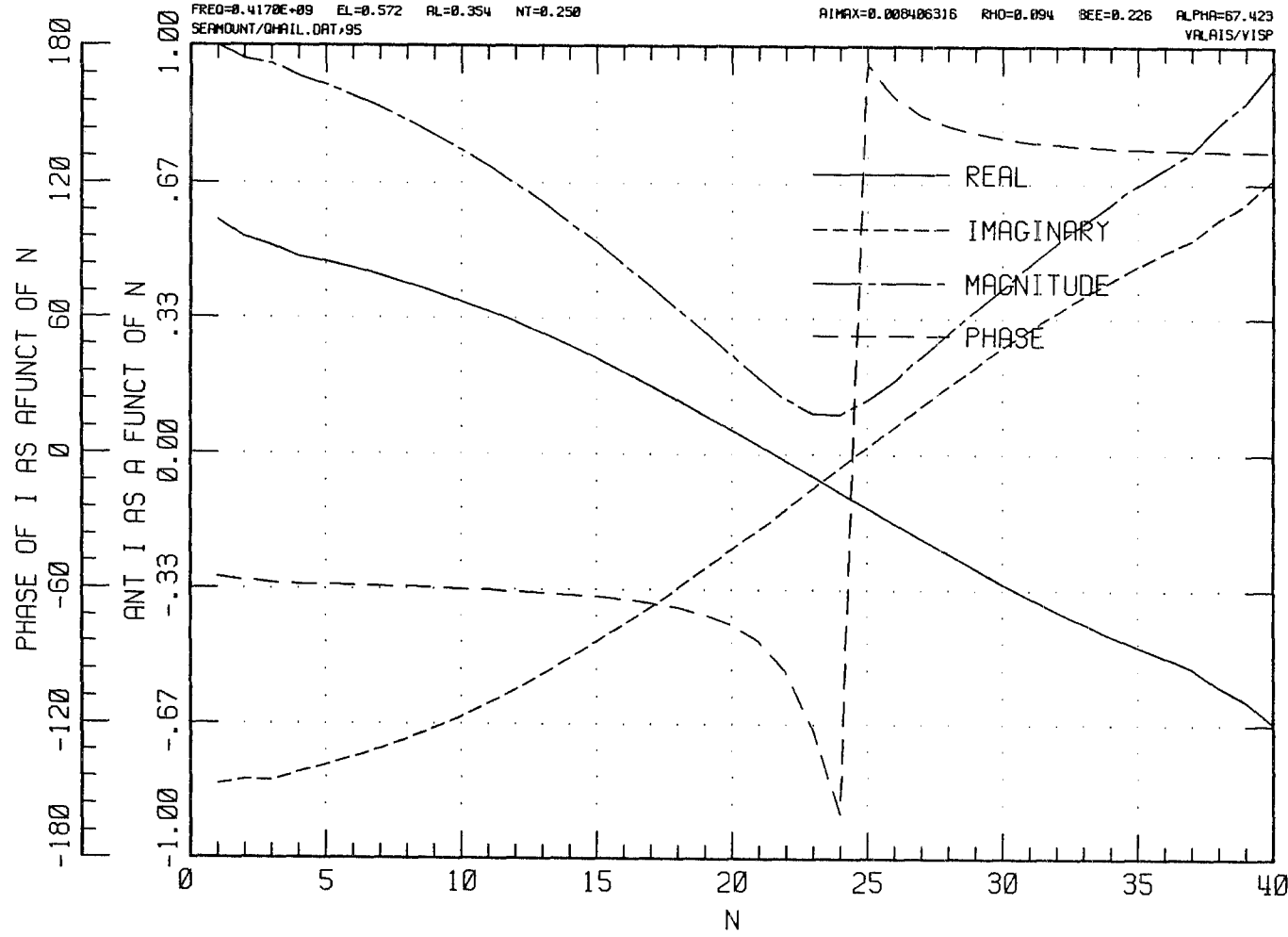
APPENDIX A  
CALCULATED CURRENT DISTRIBUTION OF THE QUADRIFILAR HELIX

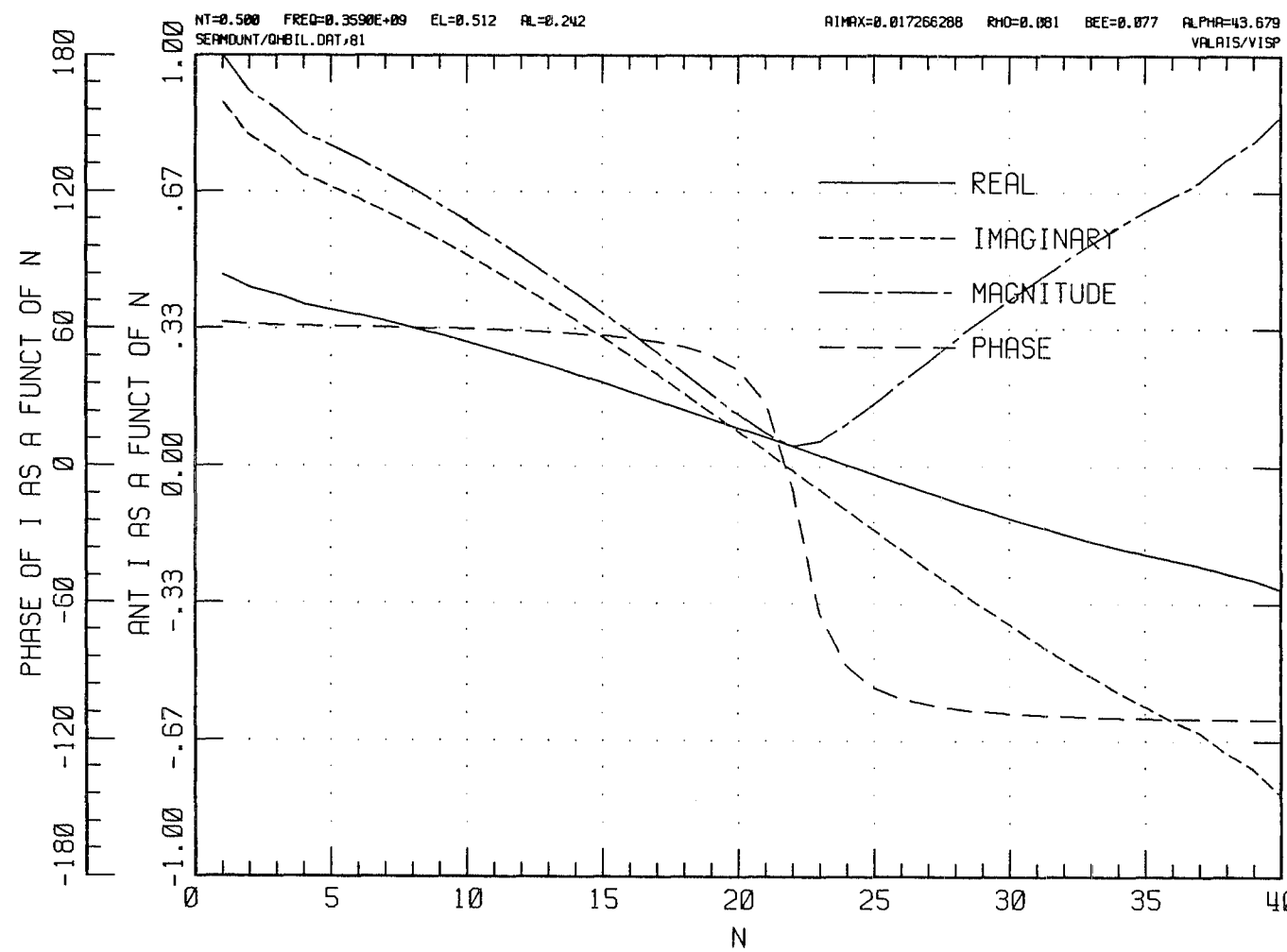
The calculated current distributions for the one-quarter turn and one-half turn fractional turn quadrifilar helices are plotted here. The distributions are as expected, sinusoidal. The maxima occur at the feed and distal ends.



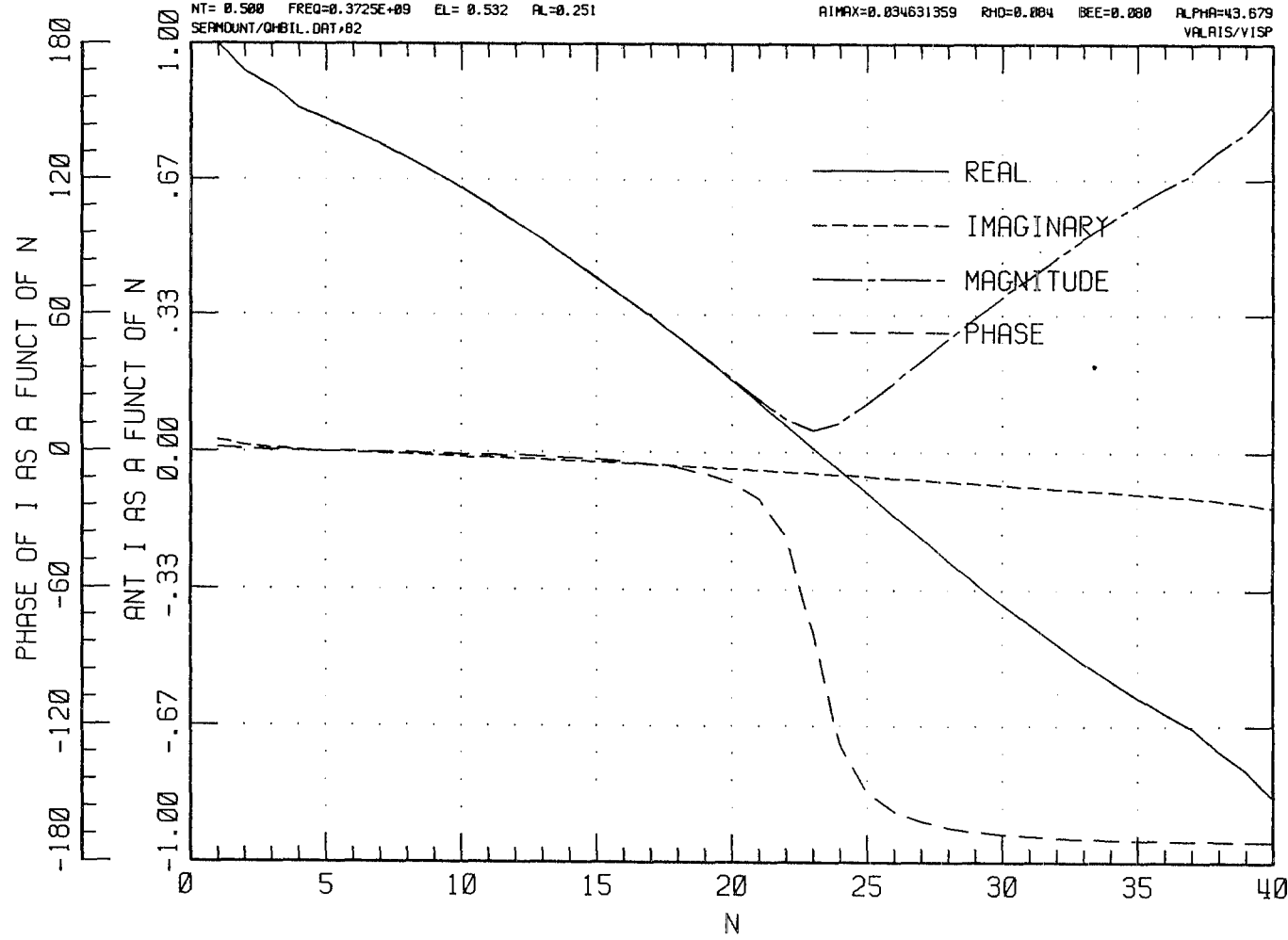


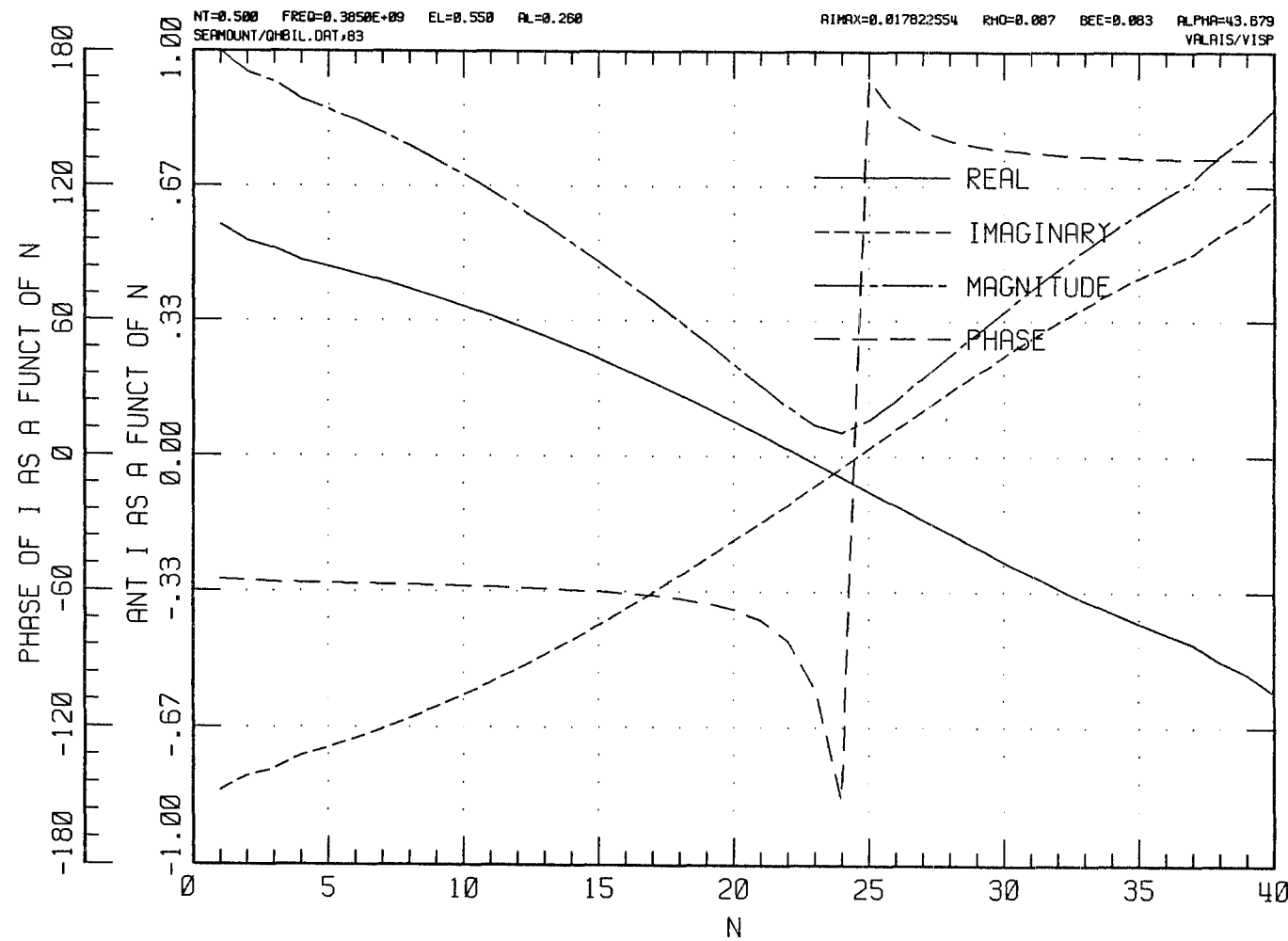


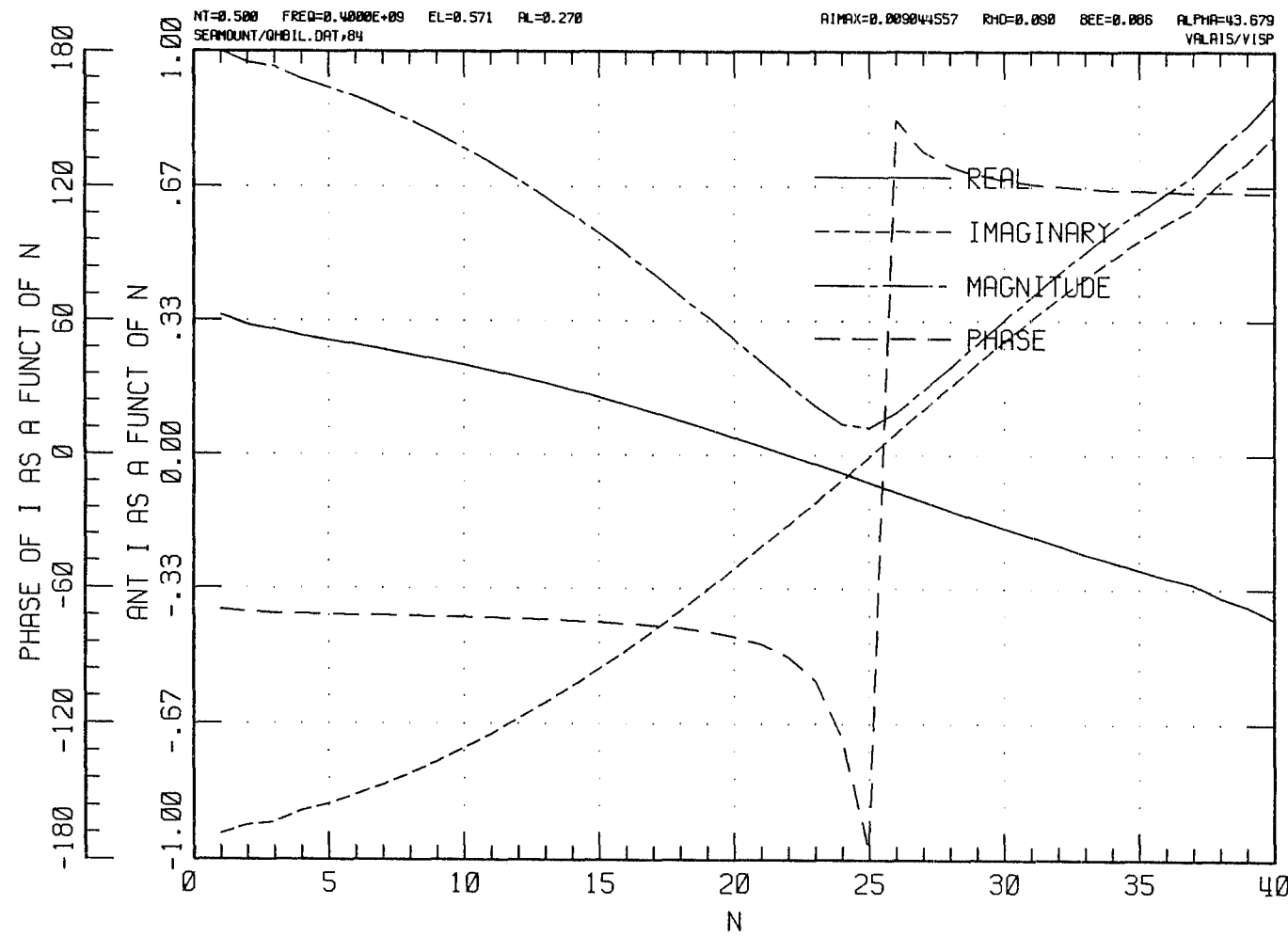


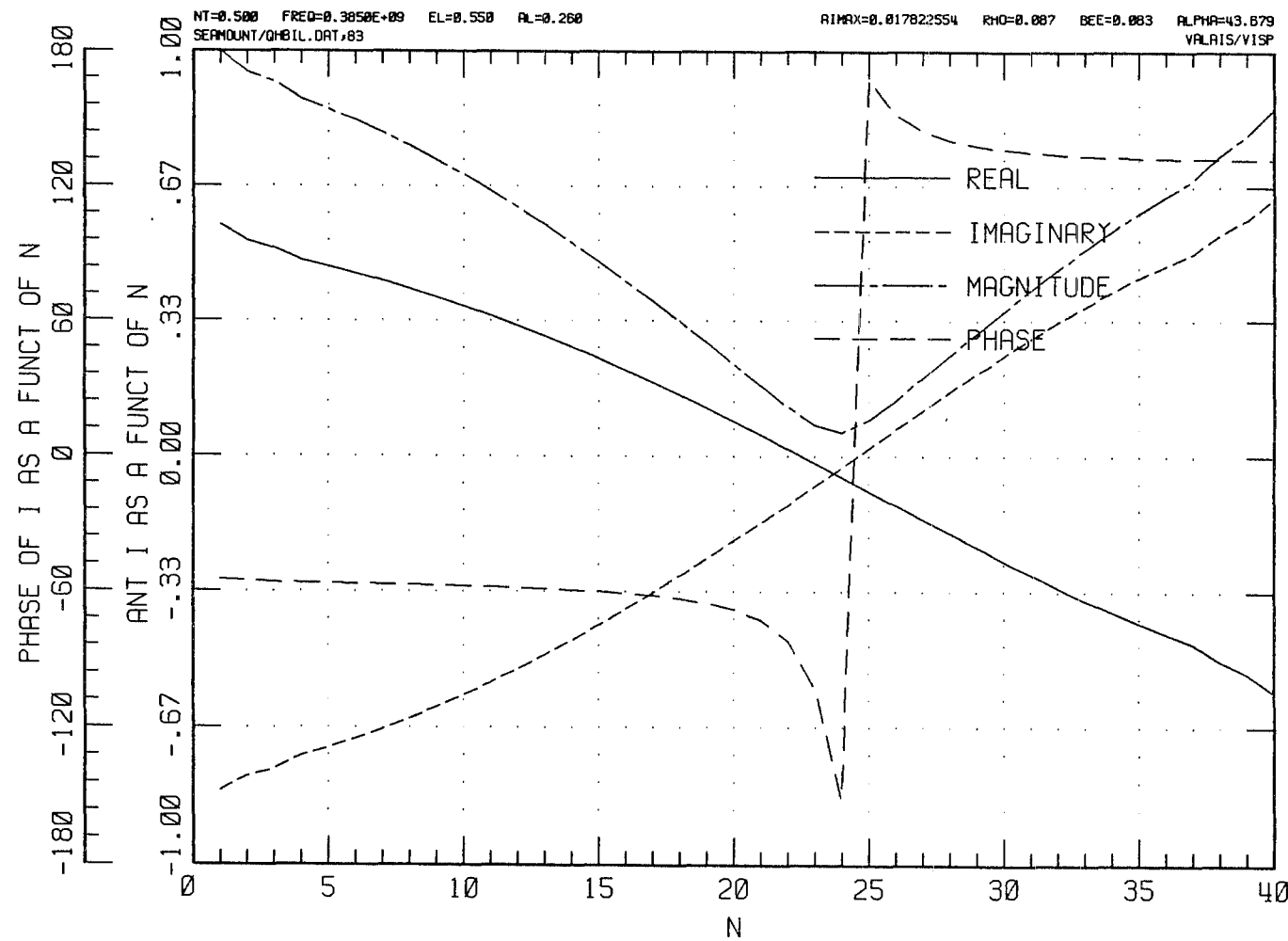


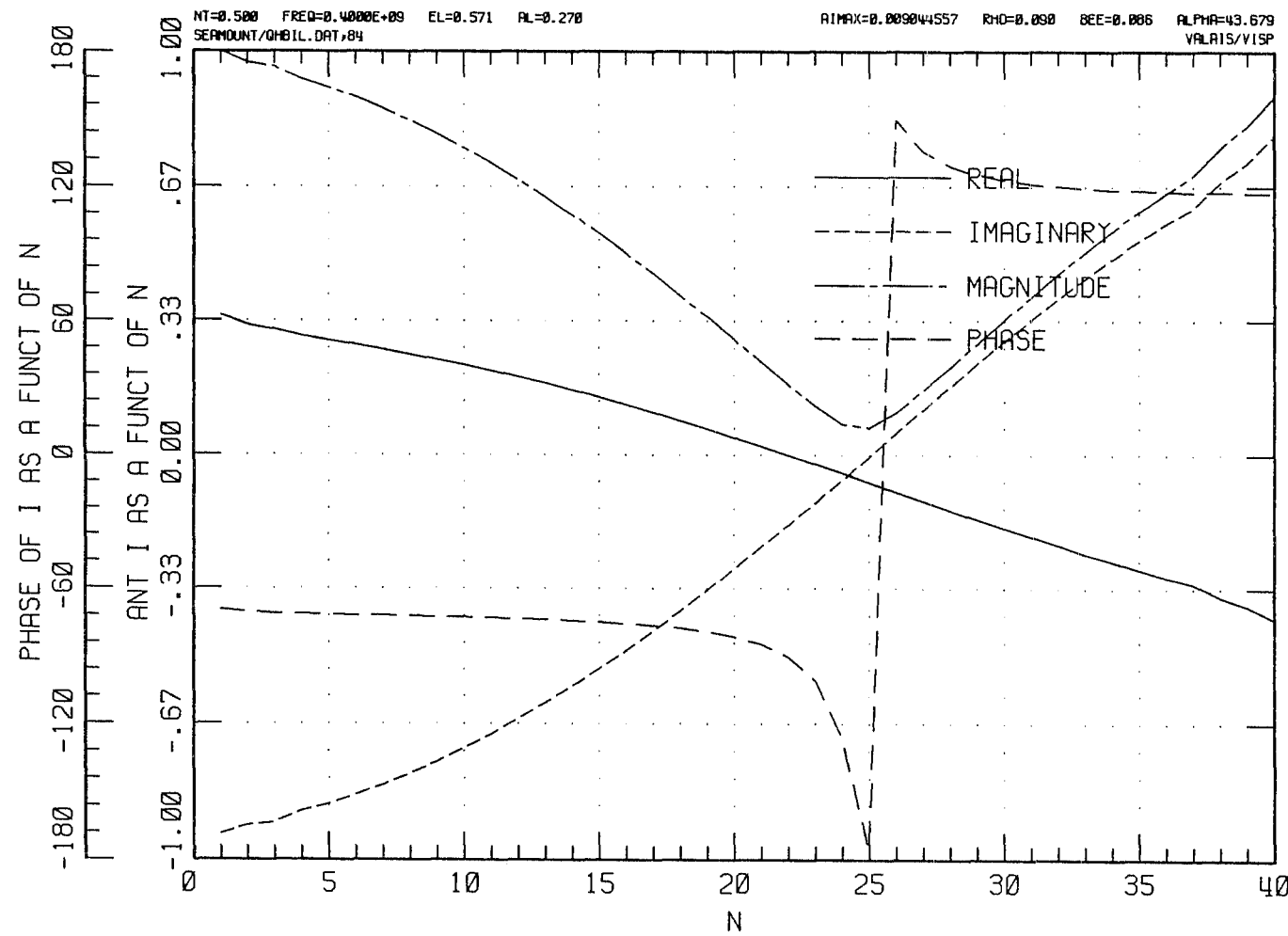
TS











APPENDIX B  
MOMENT METHOD MODEL INPUT IMPEDANCE DATA

The antenna input impedance as a function of frequency is tabulated on the following pages. These data were used to create Figures 4.1, 4.2 and 4.3.

ONE-QUARTER TURN INPUT IMPEDANCE DATA			
	RESISTANCE	REACTANCE	IMPEDANCE
0.29500E+09	66.2355	-380.9152	386.6310
0.30000E+09	64.5069	-353.0520	358.8967
0.31000E+09	61.7249	-301.9808	308.2246
0.32000E+09	59.6887	-255.8544	262.7246
0.33000E+09	58.2701	-213.4948	221.3040
0.34000E+09	57.3886	-173.9942	183.2142
0.35000E+09	56.9977	-136.6287	148.0410
0.35900E+09	57.0498	-104.3285	118.9080
0.36000E+09	57.0792	-100.7995	115.8386
0.37000E+09	57.6394	-65.9919	87.6198
0.38000E+09	58.7088	-31.7437	66.7412
0.38900E+09	60.1538	-1.0393	60.1628
0.38950E+09	60.2487	0.6698	60.2525
0.39000E+09	60.3453	2.3796	60.3922
0.40000E+09	62.6385	36.8062	72.6517
0.41000E+09	65.7197	71.9785	97.4679
0.41700E+09	68.4427	97.2966	118.9582
0.42000E+09	69.7759	108.3745	128.8942
0.43000E+09	75.0721	146.5313	164.6428
0.44000E+09	81.9854	187.0737	204.2502
0.45000E+09	91.0598	230.7483	248.0658
0.46000E+09	103.0929	278.4662	296.9370
0.47000E+09	119.2791	331.3524	352.1675
0.48000E+09	141.4503	390.7941	415.6058
0.49000E+09	172.4922	458.4597	489.8356
0.50000E+09	217.0766	536.1964	578.4711
0.51000E+09	282.9558	625.5347	686.5549
0.52000E+09	383.1632	726.0149	820.9212
0.53000E+09	539.1112	830.1558	989.8483
0.54000E+09	781.4290	909.9227	1199.4126
0.55000E+09	1131.2649	889.6203	1439.1610
0.56000E+09	1520.1107	640.8811	1649.6864
0.57000E+09	1712.0394	142.0018	1717.9184
0.58000E+09	1560.9435	-343.6060	1598.3146
0.59000E+09	1245.1763	-599.6586	1382.0472
0.60000E+09	955.1057	-667.1328	1165.0292
0.61000E+09	741.0822	-645.0652	982.5028
0.62000E+09	591.7990	-591.1624	836.4801
0.63000E+09	487.6336	-529.9426	720.1568
0.64000E+09	413.5777	-470.4679	626.4077
0.65000E+09	359.7125	-415.5687	549.6276
0.66000E+09	319.6761	-365.7055	485.7297
0.67000E+09	289.3631	-320.4980	431.7985
0.68000E+09	266.0762	-279.3190	385.7663

0.69000E+09	248.0064	-241.5178	346.1763
0.70000E+09	233.9166	-206.4971	312.0225
0.71000E+09	222.9480	-173.7319	282.6457
0.72000E+09	214.4992	-142.7664	257.6668
0.73000E+09	208.1500	-113.2040	236.9421
0.74000E+09	203.6127	-84.6954	220.5254
0.75000E+09	200.7020	-56.9273	208.6193
0.76000E+09	199.3160	-29.6130	201.5039
0.77000E+09	199.4275	-2.4839	199.4430
0.78000E+09	201.0813	24.7168	202.5947
0.79000E+09	204.3987	52.2389	210.9686
0.80000E+09	209.5893	80.3273	224.4552
0.81000E+09	216.9703	109.2194	242.9094
0.82000E+09	226.9967	139.1357	266.2447
0.83000E+09	240.3042	170.2577	294.5060
0.84000E+09	257.7686	202.6829	327.9100
0.85000E+09	280.5815	236.3376	366.8534

## ONE-HALF TURN INPUT IMPEDANCE DATA

	RESISTANCE	REACTANCE	IMPEDANCE
0.29500E+09	30.1380	-331.9528	333.3181
0.30000E+09	29.3254	-304.6005	306.0089
0.31000E+09	27.9861	-254.0573	255.5940
0.32000E+09	27.0056	-207.8746	209.6215
0.33000E+09	26.3828	-164.9304	167.0272
0.34000E+09	26.1430	-124.3453	127.0638
0.35000E+09	26.3388	-85.4039	89.3731
0.35900E+09	26.9556	-51.2611	57.9163
0.36000E+09	27.0536	-47.5021	54.6657
0.37000E+09	28.4080	-10.1094	30.1531
0.37250E+09	28.8649	-0.7834	28.8756
0.37500E+09	29.3752	8.5483	30.5938
0.38000E+09	30.5697	27.2572	40.9569
0.38500E+09	32.0222	46.0735	56.1087
0.39000E+09	33.7684	65.0520	73.2944
0.40000E+09	38.3151	103.7125	110.5637
0.41000E+09	44.6314	143.6641	150.4372
0.42000E+09	53.2865	185.3146	192.8236
0.43000E+09	65.0488	229.0330	238.0913
0.44000E+09	80.9507	275.1017	286.7647
0.44500E+09	90.8676	299.0609	312.5609
0.45000E+09	102.3656	323.6251	339.4288
0.46000E+09	131.0854	374.3654	396.6521
0.47000E+09	169.3618	426.4696	458.8679
0.48000E+09	219.8295	478.0485	526.1705
0.49000E+09	285.1508	525.6134	597.9803
0.50000E+09	367.1364	563.5188	672.5642
0.51000E+09	465.1365	583.8780	746.5022
0.52000E+09	573.9474	577.8093	814.4195
0.53000E+09	682.5500	538.7331	869.5447
0.54000E+09	775.8802	466.8253	905.4921
0.55000E+09	840.3508	371.2656	918.7097
0.56000E+09	869.8367	267.2676	909.9714
0.57000E+09	867.3182	169.6081	883.7465
0.58000E+09	841.5297	87.7102	846.0882
0.59000E+09	802.2502	24.8494	802.6350
0.60000E+09	757.3565	-19.9336	757.6188
0.61000E+09	712.0422	-49.5372	713.7633
0.62000E+09	669.2330	-67.2504	672.6034
0.63000E+09	630.3094	-76.0111	634.8761
0.64000E+09	595.7302	-78.1755	600.8377
0.65000E+09	565.4589	-75.5285	570.4808
0.66000E+09	539.2245	-69.3797	543.6695
0.66500E+09	527.5099	-65.2986	531.5361

0.67000E+09	516.6681	-60.6725	520.2183
0.68000E+09	497.4212	-50.0775	499.9356
0.69000E+09	481.1437	-38.0671	482.6472
0.70000E+09	467.5410	-24.9699	468.2073
0.71000E+09	456.3700	-11.0107	456.5028
0.72000E+09	447.4406	3.6609	447.4556
0.73000E+09	440.6146	18.9499	441.0219
0.74000E+09	435.8051	34.8008	437.1924
0.75000E+09	432.9775	51.1863	435.9926
0.76000E+09	432.1515	68.0973	437.4839
0.77000E+09	433.4062	85.5349	441.7660
0.78000E+09	436.8886	103.4996	448.9808
0.79000E+09	442.8250	121.9790	459.3179
0.80000E+09	451.5382	140.9286	473.0197
0.81000E+09	463.4684	160.2423	490.3881
0.82000E+09	479.1989	179.7050	511.7865
0.83000E+09	499.4819	198.9158	537.6334
0.84000E+09	525.2526	217.1647	568.3755
0.85000E+09	557.6033	233.2387	604.4185

## ONE TURN INPUT IMPEDANCE DATA

	RESISTANCE	REACTANCE	IMPEDANCE
0.28500E+09	-7.9213	-508.8395	508.9012
0.29000E+09	-7.8426	-468.8374	468.9030
0.30000E+09	-7.7871	-399.7140	399.7899
0.31000E+09	-7.8378	-341.5548	341.6448
0.32000E+09	-7.9713	-291.3908	291.4998
0.33000E+09	-8.1727	-247.1882	247.3233
0.34000E+09	-8.4317	-207.4990	207.6703
0.35000E+09	-8.7412	-171.2557	171.4787
0.36000E+09	-9.0952	-137.6449	137.9451
0.37000E+09	-9.4886	-106.0261	106.4498
0.38000E+09	-9.9160	-75.8774	76.5226
0.39000E+09	-10.3710	-46.7577	47.8941
0.40000E+09	-10.8452	-18.2786	21.2539
0.40600E+09	-11.1343	-1.3492	11.2157
0.40700E+09	-11.1825	1.4677	11.2784
0.41000E+09	-11.3270	9.9173	15.0550
0.41250E+09	-11.4469	16.9625	20.4635
0.41500E+09	-11.5659	24.0168	26.6566
0.41750E+09	-11.6837	31.0858	33.2089
0.42000E+09	-11.8000	38.1747	39.9568
0.43000E+09	-12.2403	66.8426	67.9541
0.44000E+09	-12.6131	96.2916	97.1142
0.45000E+09	-12.8673	126.9336	127.5841
0.46000E+09	-12.9262	159.2455	159.7693
0.47000E+09	-12.6745	193.8009	194.2149
0.48000E+09	-11.9357	231.3123	231.6200
0.49000E+09	-10.4344	272.6924	272.8920
0.50000E+09	-7.7315	319.1432	319.2369
0.51000E+09	-3.1085	372.2893	372.3023
0.52000E+09	4.6490	434.3813	434.4062
0.53000E+09	17.6729	508.6064	508.9133
0.54000E+09	39.8774	599.5451	600.8699
0.55000E+09	78.8332	713.7518	718.0921
0.56000E+09	150.0452	859.9959	872.9871
0.57000E+09	286.9435	1046.4557	1085.0835
0.58000E+09	561.7662	1261.4688	1380.9000
0.59000E+09	1096.0979	1386.5643	1767.4816
0.60000E+09	1832.7821	1033.6620	2104.1738
0.61000E+09	2052.6047	121.1800	2056.1787
0.62000E+09	1614.4719	-488.8018	1686.8452
0.63000E+09	1153.2682	-642.2797	1320.0571
0.64000E+09	847.0253	-616.9701	1047.9046
0.65000E+09	655.2177	-547.3870	853.7814

0.66000E+09	531.7158	-474.1834	712.4406
0.67000E+09	448.8423	-407.6508	606.3320
0.68000E+09	391.1158	-349.3656	524.4310
0.69000E+09	349.6997	-298.5825	459.8276
0.70000E+09	319.3454	-254.0998	408.1032
0.71000E+09	296.8035	-214.7847	366.3670
0.71500E+09	287.7780	-196.7626	348.6140
0.72000E+09	279.9841	-179.6945	332.6878
0.73000E+09	267.4966	-148.0774	305.7472
0.74000E+09	258.3882	-119.3438	284.6180
0.75000E+09	251.9883	-93.0335	268.6138
0.76000E+09	247.8138	-68.7880	257.1837
0.77000E+09	245.5084	-46.3282	249.8413
0.78000E+09	244.8036	-25.4374	246.1216
0.79000E+09	245.4920	-5.9474	245.5640
0.80000E+09	247.4092	12.2711	247.7133
0.81000E+09	250.4207	29.3173	252.1310
0.82000E+09	254.4131	45.2667	258.4088
0.83000E+09	259.2874	60.1762	266.1787
0.84000E+09	264.9537	74.0893	275.1176
0.85000E+09	271.3289	87.0394	284.9478
0.85500E+09	274.7574	93.1619	290.1220

APPENDIX C  
ONE-QUARTER AND ONE-HALF TURN QUADRIFILAR HELIX  
RADIATION PATTERNS

The far field electric field radiation pattern are plotted for one-quarter turn and one-half turn quadrifilar antennas. The patterns show the magnitudes of the  $E_\theta$ ,  $E_\phi$  and total fields in the  $\phi = 0^\circ$  and  $\phi = 90^\circ$  planes. The frequencies plotted are the upper and lower impedance bandwidth boundaries, resonance and 400 MHz.

NT= 0.250      RL= 0.305  
SEAMOUNT/EBL.DAT,21

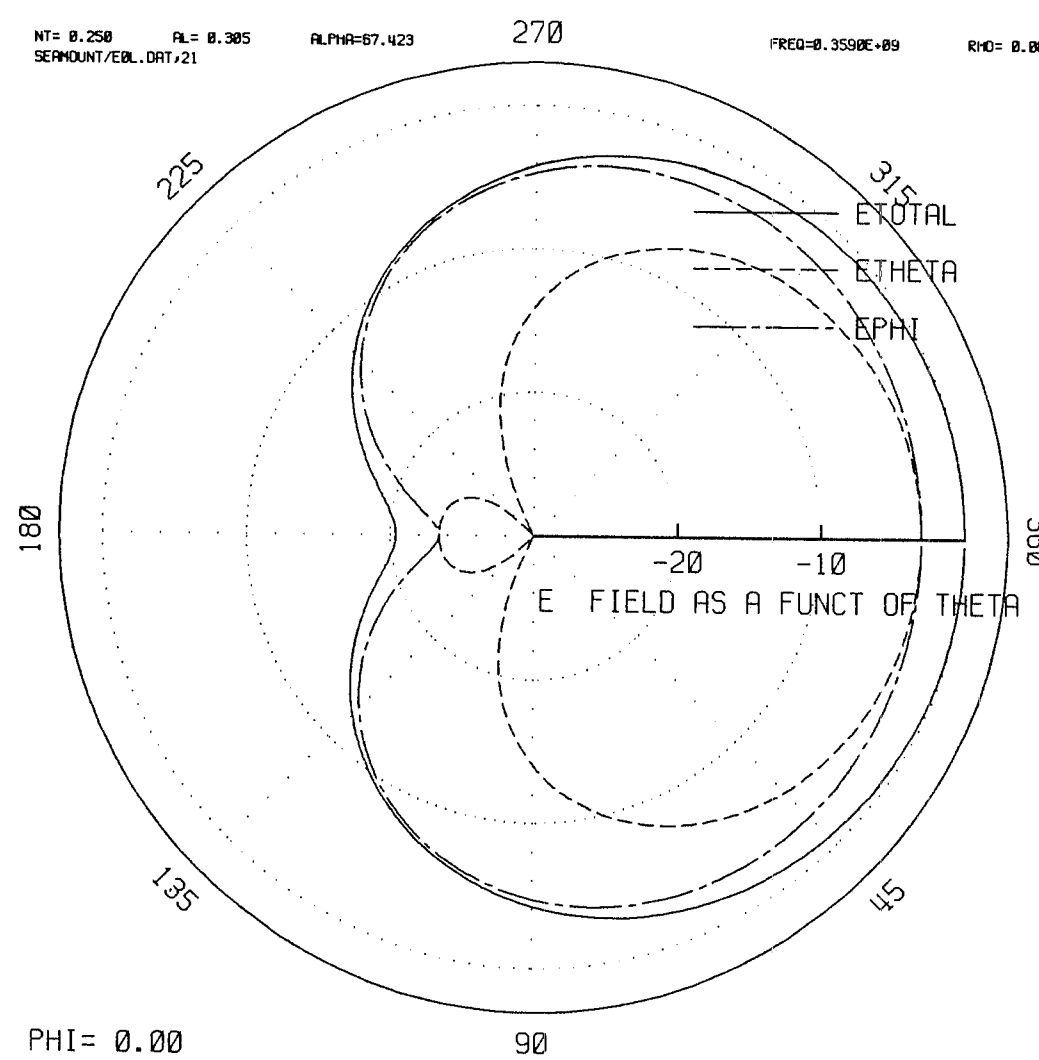
ALPHA=67.423

270

FREQ=0.3590E+09

RHO= 0.001

BEE= 0.194  
VALRIS/VISP



NT= 0.250      RL= 0.331  
SEAMOUNT/E0L.DAT/22

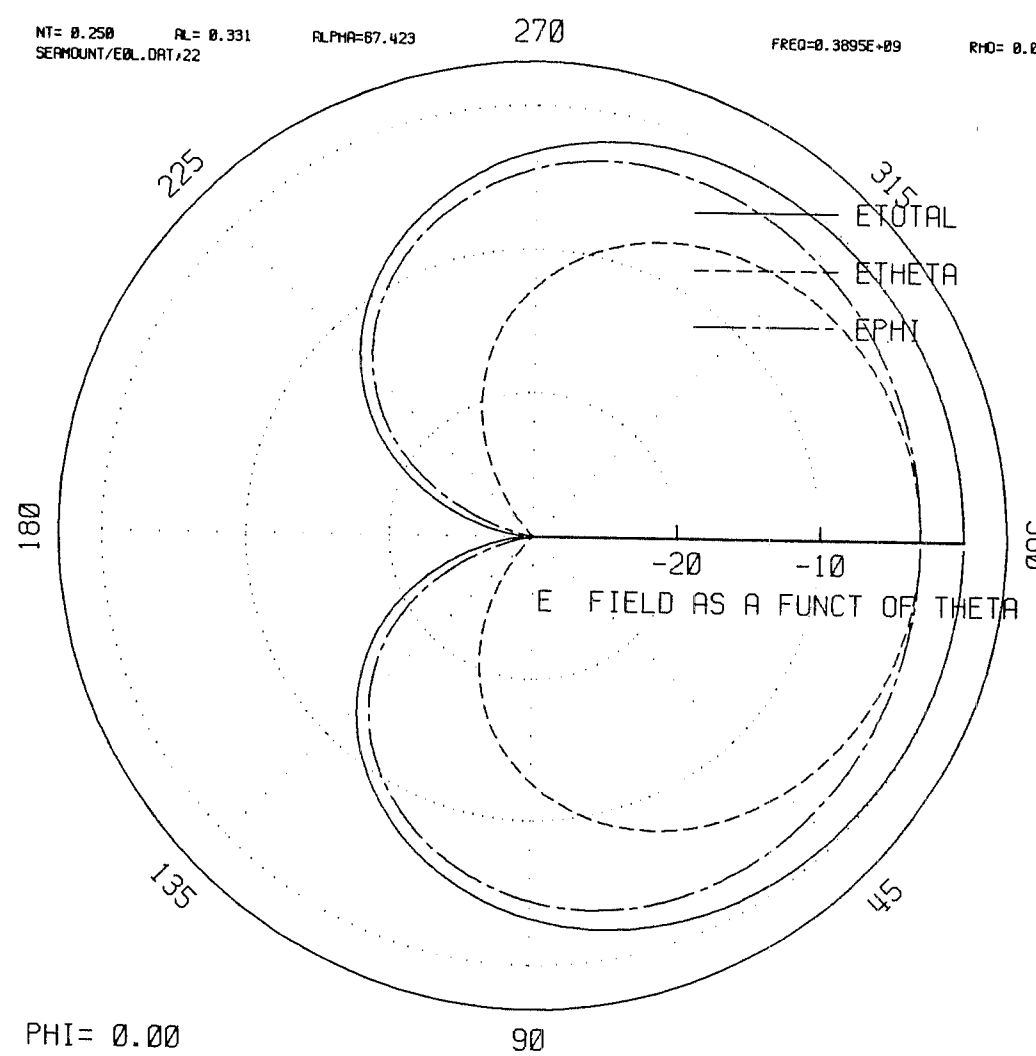
ALPHA=67.423

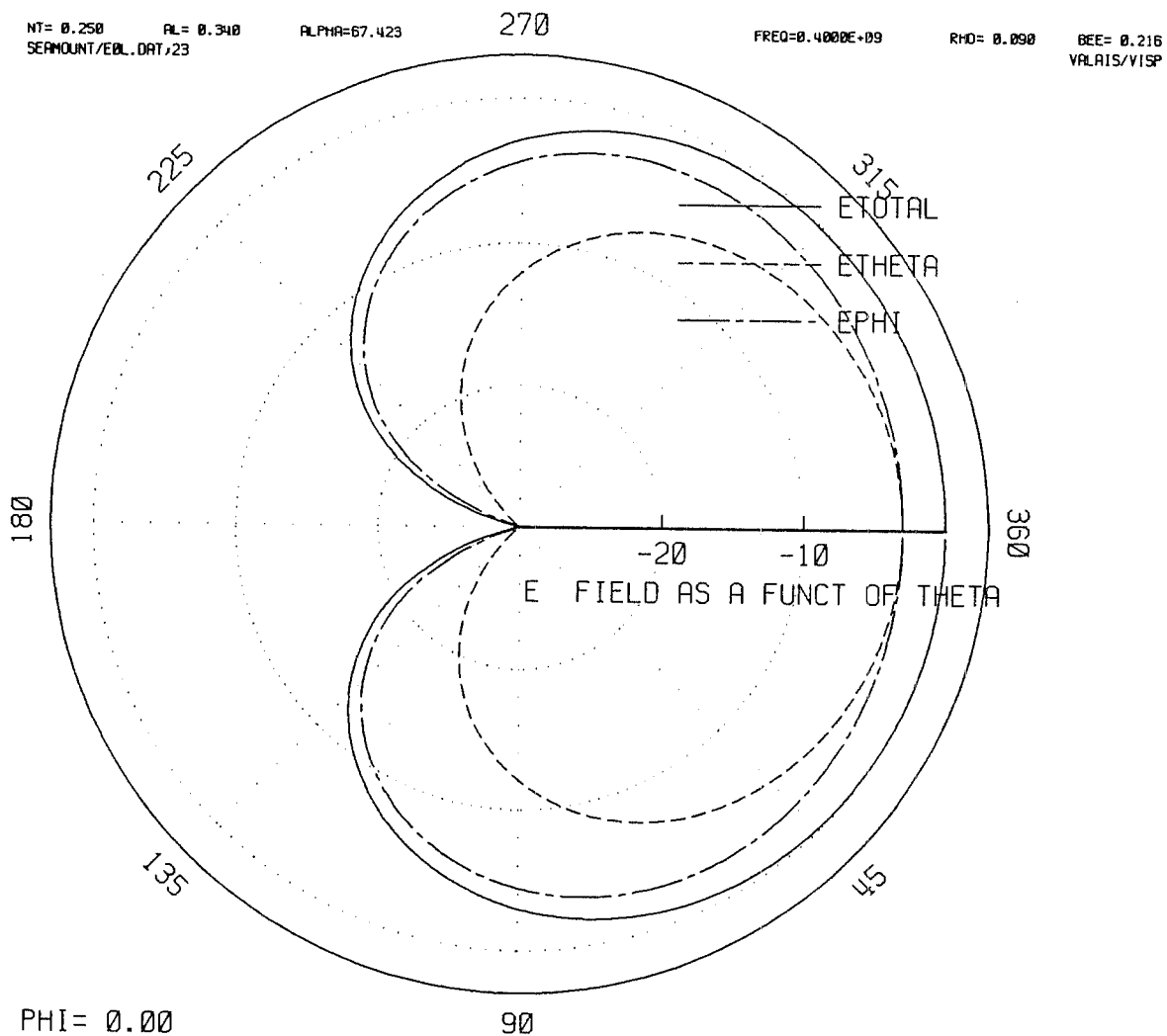
270

FREQ=0.3895E+09

RHO= 0.088

BEE= 0.211  
VALRIS/Y1SP





NT= 0.250      AL= 0.354  
SEAMOUNT/EBL.DAT,24

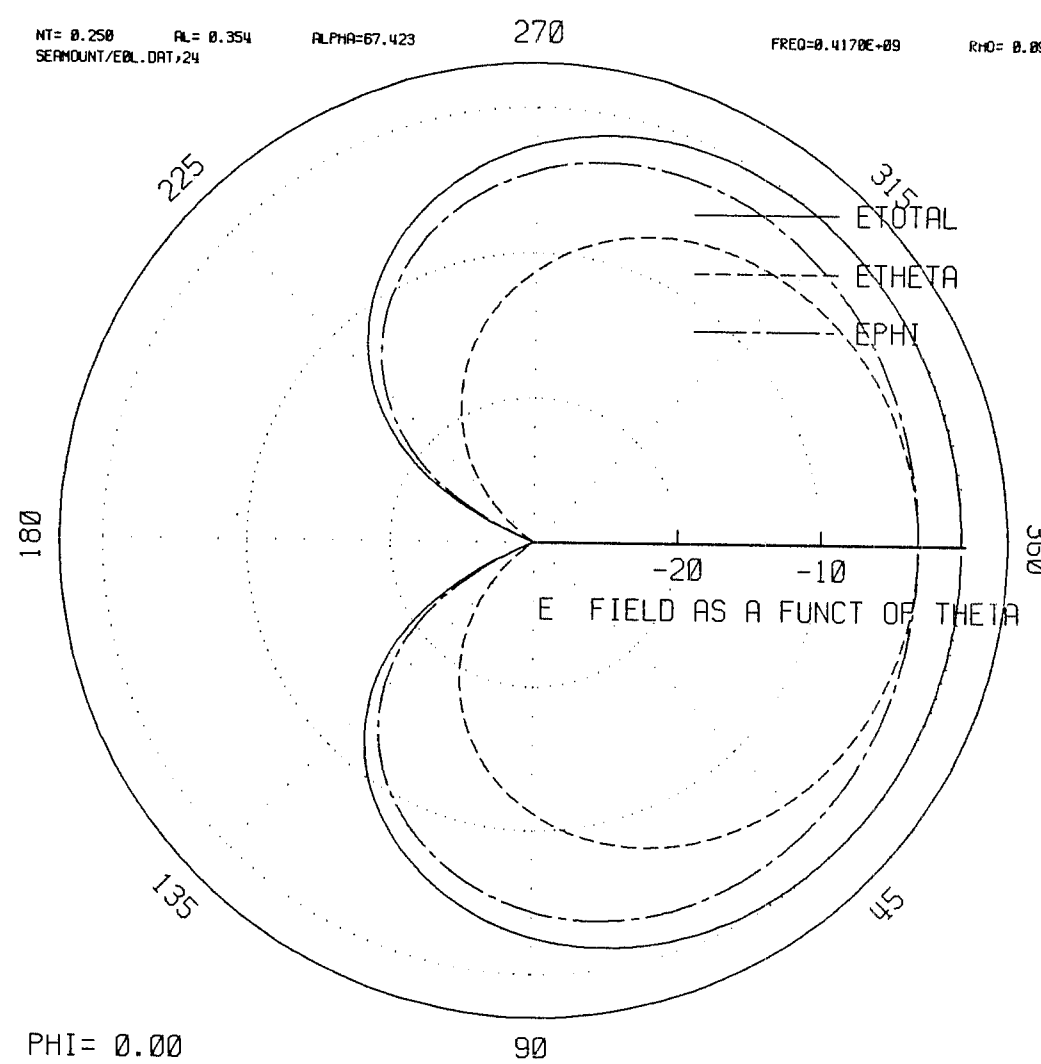
ALPHA=67.423

270

FREQ=0.4170E+09

RHO= 0.894

BEE= 0.226  
VRLAIS/VISP



NT= 0.500      RL= 0.242  
SERMOUNT/EBL.DAT,25

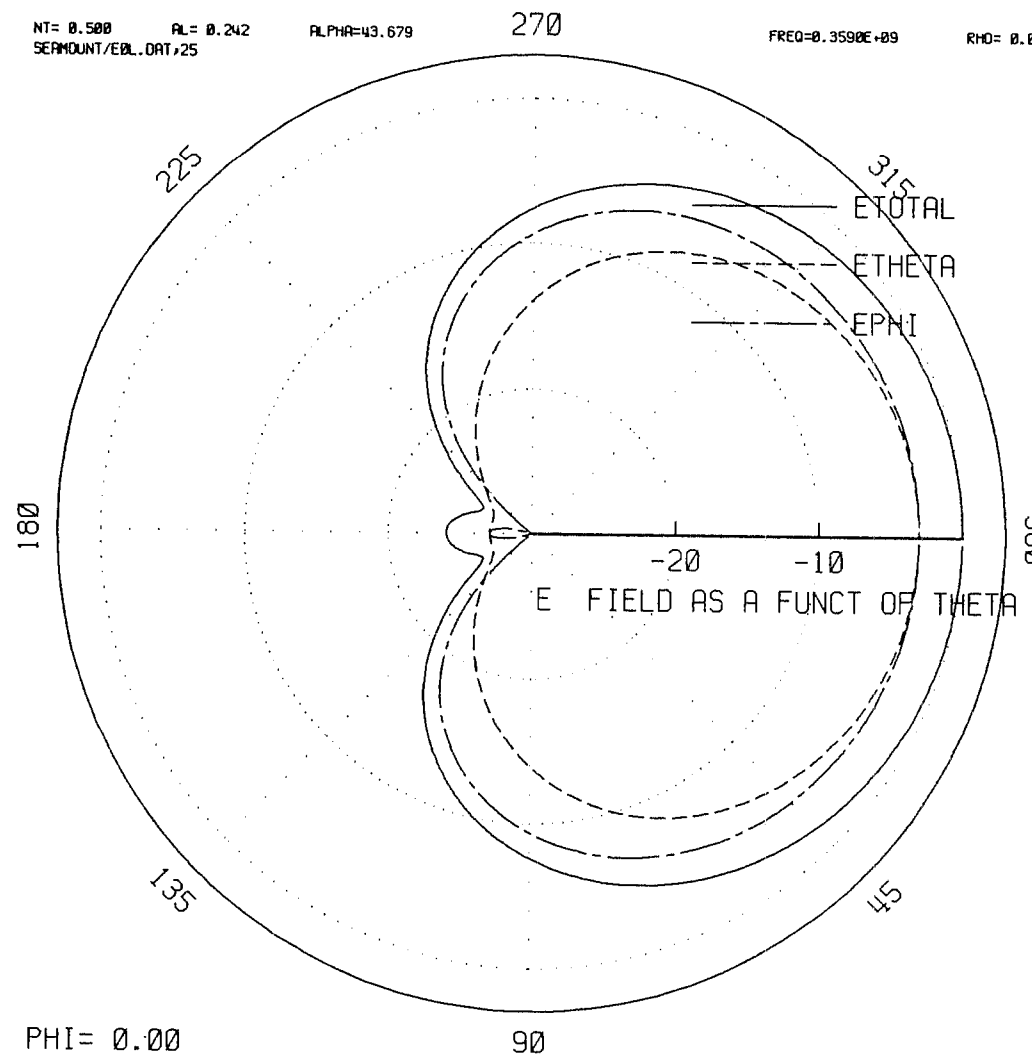
ALPHA=43.679

270

FREQ=0.3590E+09

RHO= 0.081

BEE= 0.077  
VALRIS/VISP



NT= 0.500  
SERMOUNT/EBL.DAT,26

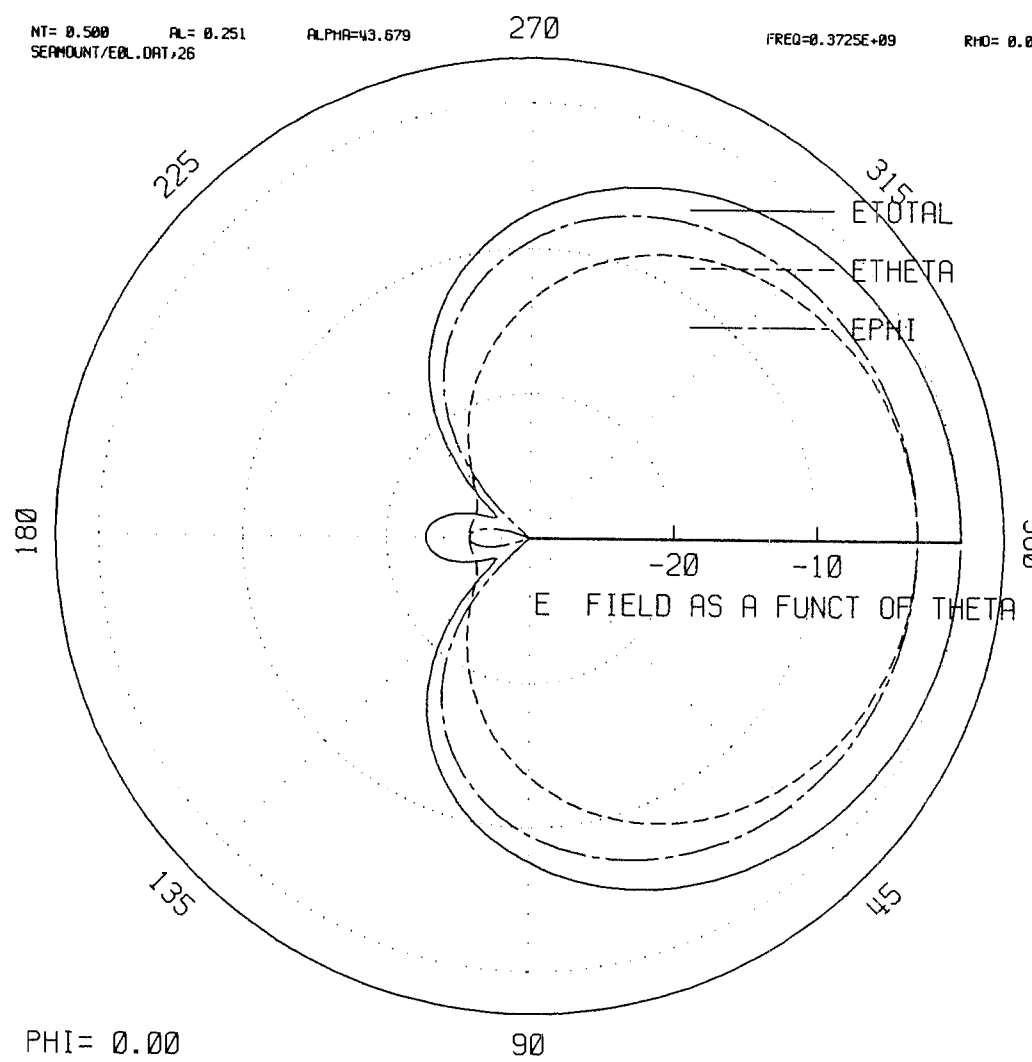
ALPHA=43.679

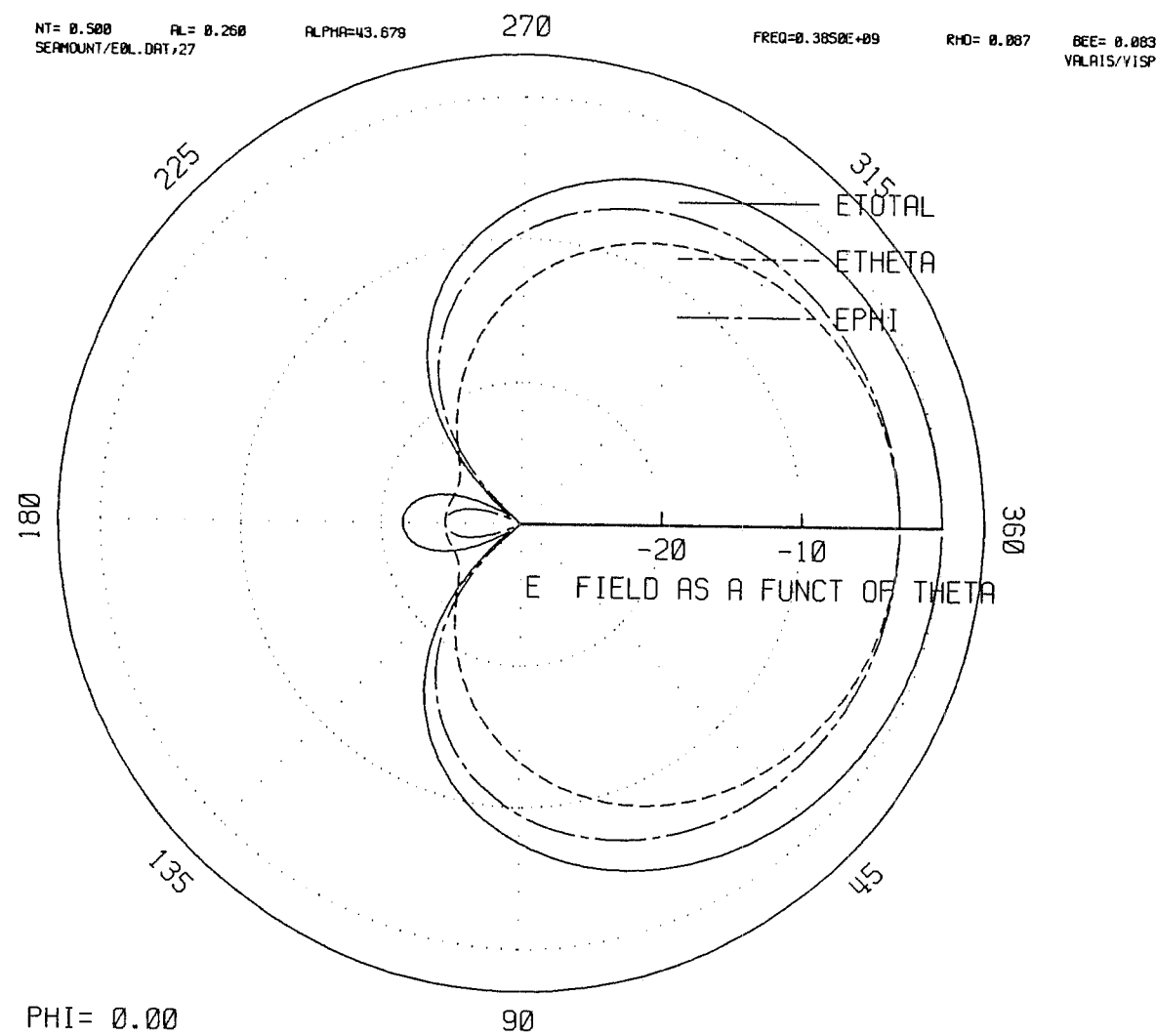
270

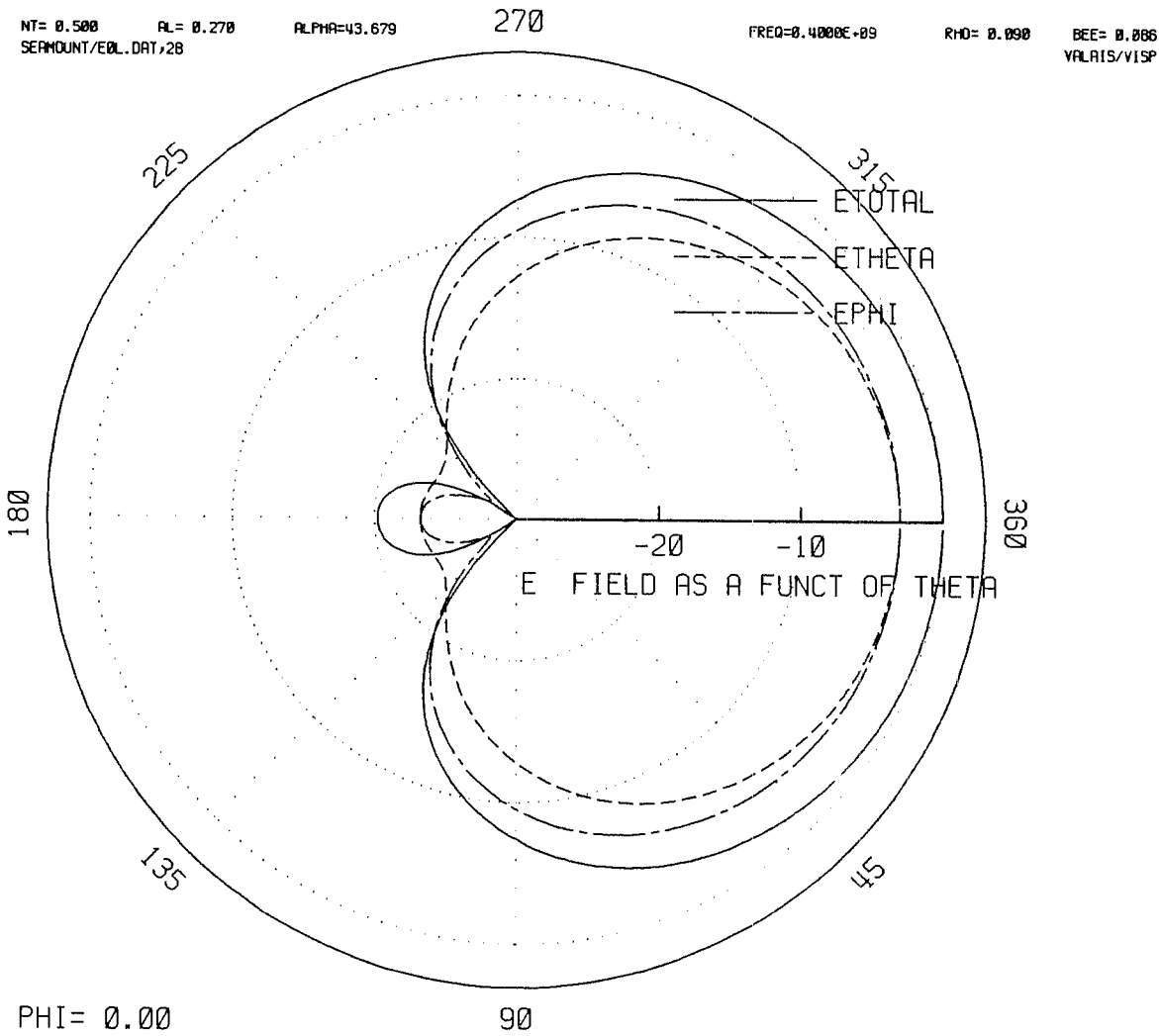
FREQ=0.3725E+09

RHO= 0.004

BEE= 0.000  
VALAIS/VISP







NT= 0.250      RL= 0.305  
SEAMOUNT/E90L.DAT,21

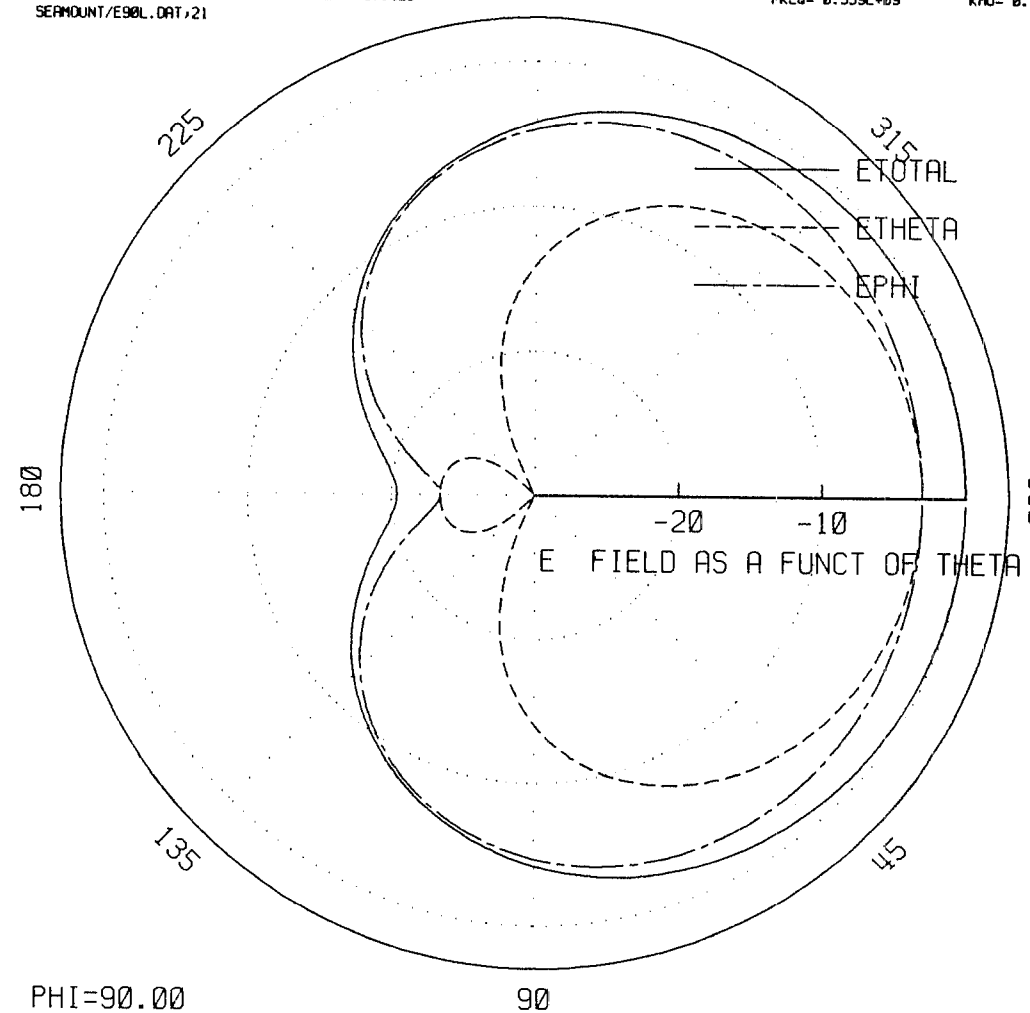
ALPHA=67.423

270

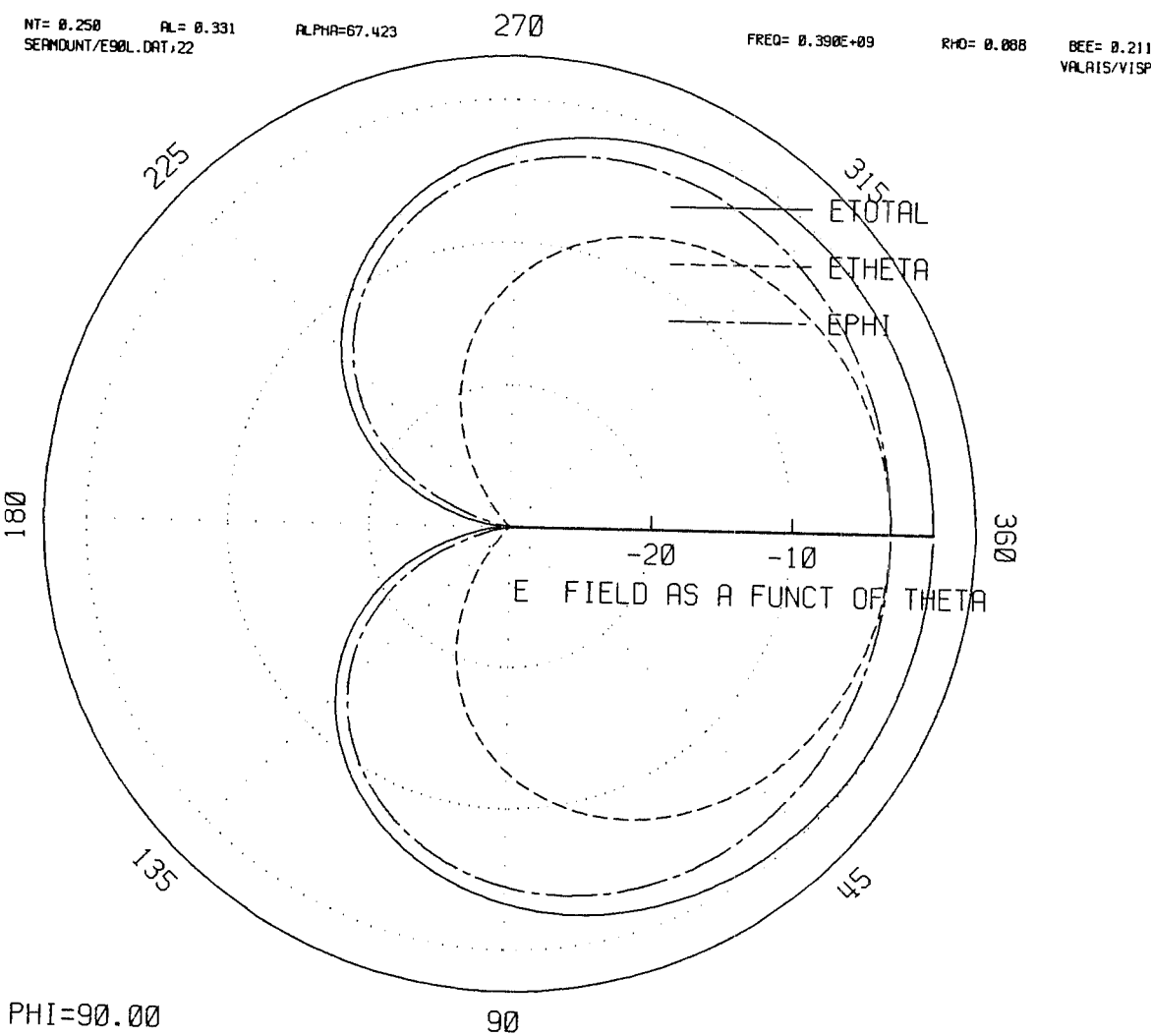
FREQ= 0.359E+09

RHO= 0.001

BEE= 0.194  
VALAIS/VISP



71



NT= 0.250  
RL= 0.340  
SEAMOUNT/E90L.DAT/23

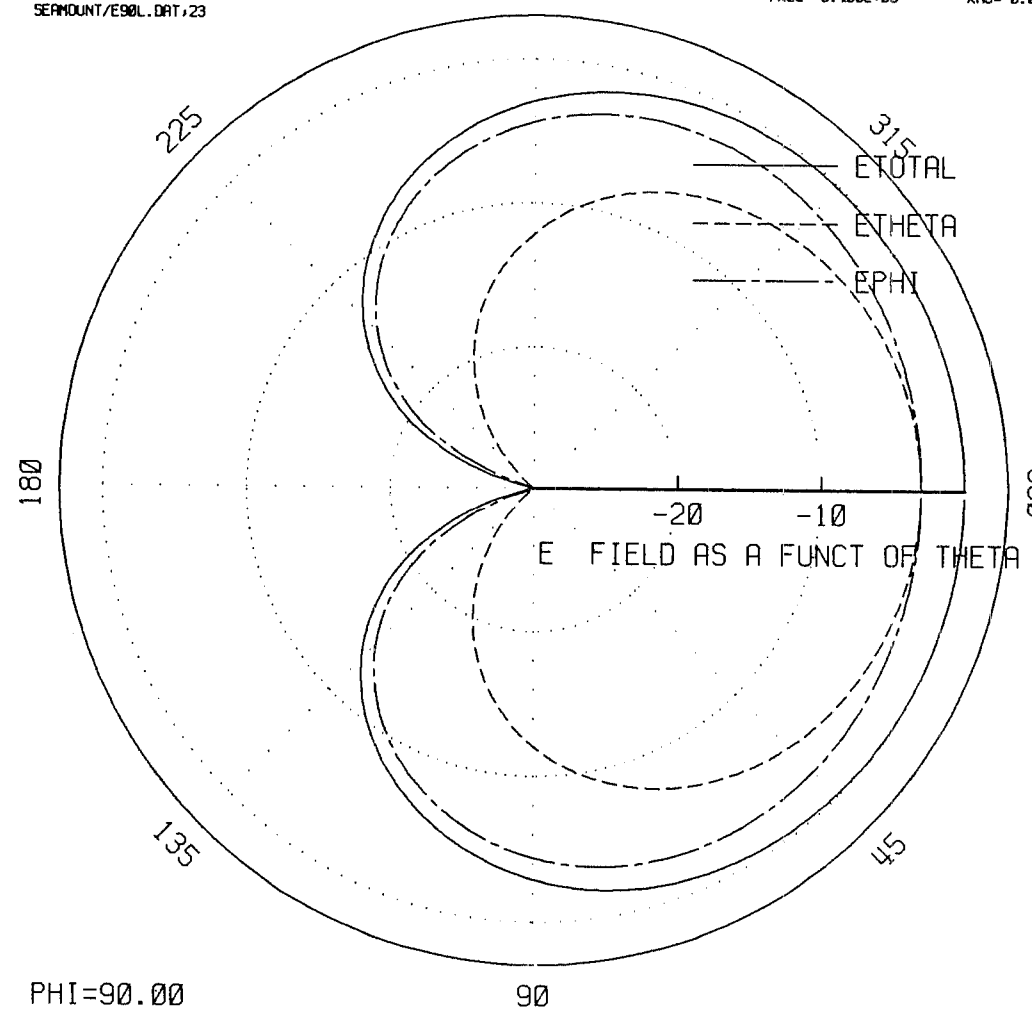
ALPHA=67.423

270

FREQ= 0.400E+09

RHO= 0.090

BEE= 0.216  
VALAIS/VISP



NT= 0.250      RL= 0.354  
SERMOUNT/E90L.DAT,24

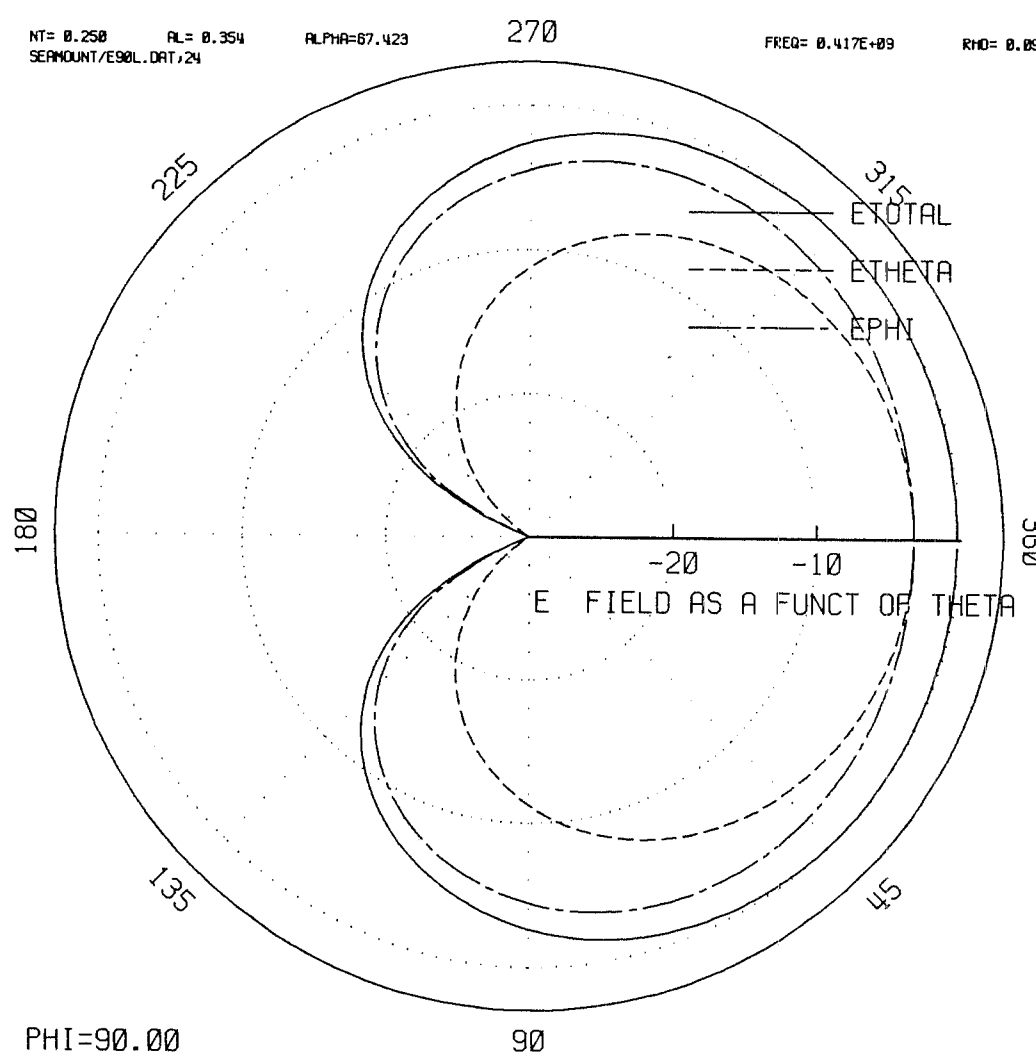
ALPHA=67.423

270

FREQ= 0.417E+09

RHO= 0.094

BEE= 0.226  
VALRIS/V1SP



NT= 0.500 RL= 0.242  
SEAMOUNT/E90L.DAT,25

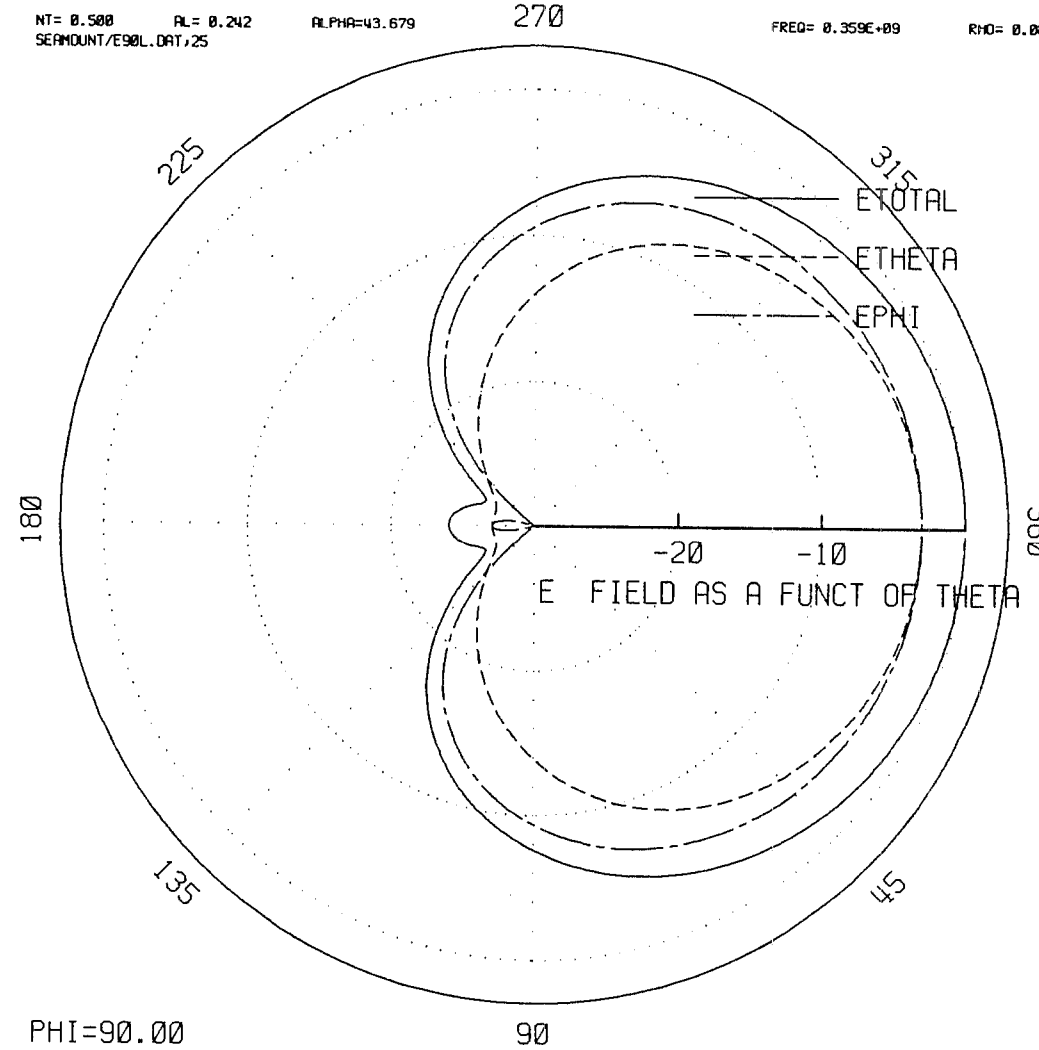
ALPHA=43.679

270

FREQ= 0.359E+09

RHO= 0.081

BEE= 0.077  
VALRIS/VISP



NT= 0.500 AL= 0.251  
SEAMOUNT/E90L.DAT,26

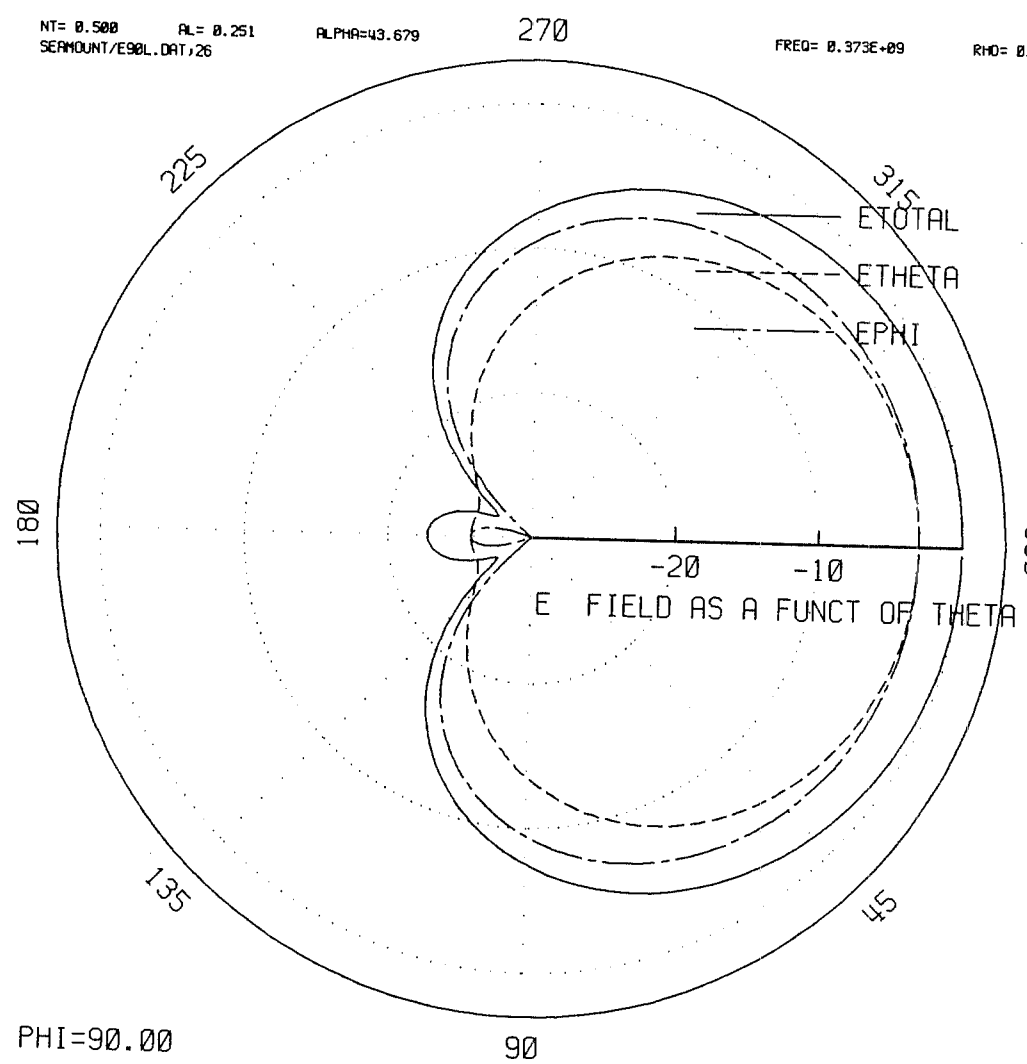
ALPHA=43.679

270

FREQ= 0.373E+09

RHD = 0.

BEE = 0.082  
VALRIS/VISA



NT= 0.500 RL= 0.260  
SEAMOUNT/E90L.DAT,27

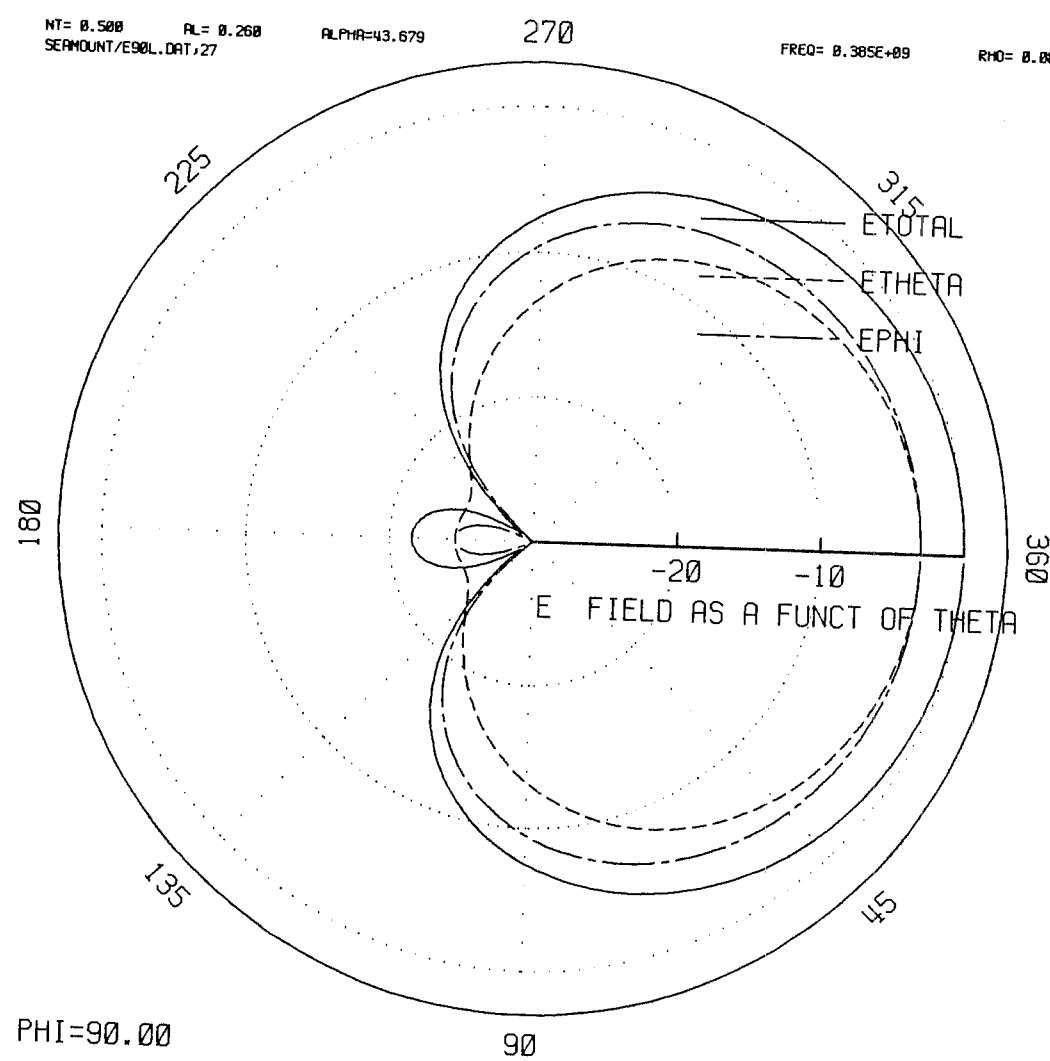
ALPHR=43.679

270

FREQ= 0.385E+09

RHO= 0.087

BEE= 0.083  
VRLAIS/VISP



NT= 0.500      RL= 0.270  
SEAMOUNT/E90L.DAT/28

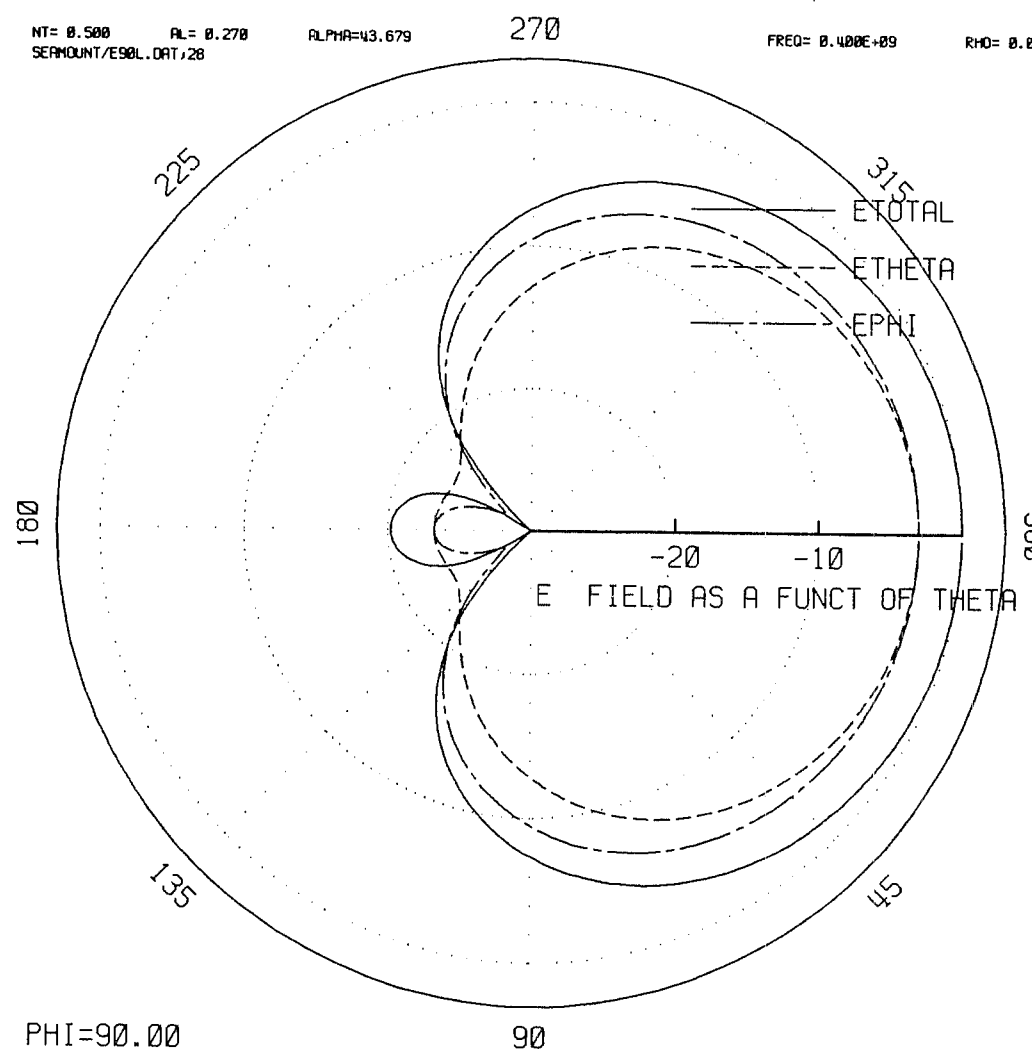
ALPHA=43.679

270

FREQ= 0.400E+09

RHO= 0.090

BEE= 0.066  
VALRIS/VISP



APPENDIX D  
POLARIZATION CHARACTERISTICS OF THE QUADRIFILAR HELIX  
RADIATED FIELD

D.1 INTRODUCTION

The polarization of the electric field, when viewed at a far field point, may be described by the polarization ellipse. Figure D.1 illustrates the polarization ellipse of the electric field. The ellipse is generated by the tip of the electric field vector as it rotates in the plane of polarization perpendicular to the direction of wave travel. The ellipse, shown, is viewed in the opposite direction of wave travel. The direction of wave travel is out of the page. The polarization ellipse and the polarization state of the electric field can be completely characterized by the axial ratio, AR, the tilt angle,  $\tau$ , and the sense of rotation, right or left. The tilt angle, axial ratio and sense of rotation can all be obtained from the magnitude of the orthogonal  $\theta$  and  $\phi$  electric field components and their respective phases,  $\delta_\theta$  and  $\delta_\phi$ .

## D.2 THE POLARIZATION CHARACTERISTICS

The linear polarization ratio,  $p_\ell$ , is defined as

$$p_\ell = \frac{E_\phi}{E_\theta} = |p_\ell| e^{j\delta}$$

where  $\delta$  is the phase difference,

$$\delta = \delta_\phi - \delta_\theta$$

of the two field components  $E_\phi$  and  $E_\theta$ . An auxillary angle,  $\alpha_a$ , is also defined such that

$$\tan \alpha_a = \frac{|E_\phi|}{|E_\theta|} = |p_\ell|$$

The tilt angle,  $\tau$ , of the ellipse can be determined from the phase difference and polarization ratio

$$\tan 2\tau = \frac{2|p_\ell| \cos \delta}{1 - |p_\ell|^2}$$

or by noting that

$$\frac{2|p_\ell|}{1 - |p_\ell|^2} = \tan 2\alpha_a$$

can be rewritten as

$$\tan 2\tau = \tan 2\alpha_a \cos \delta$$

The angle,  $\xi$ , sometimes called the ellipticity angle, is related to the axial ratio by

$$\tan \xi = \pm \frac{n}{m} = \pm \frac{1}{AR}$$

and

$$\sin 2\xi = \sin 2\alpha_a \sin \delta$$

One can determine the axial ratio of the ellipse by solving for the ellipticity,  $\xi$ ,

$$AR = \frac{1}{\tan \xi} = \{\tan[1/2 \sin^{-1}(\sin 2\alpha_a \sin \delta)]\}^{-1}$$

The sign of the axial ratio determines the polarization sense + for right hand and - for left hand rotation. The axial ratios for the one-quarter and one-half turn quadrifilar helices considered here were positive indicating right hand sense.

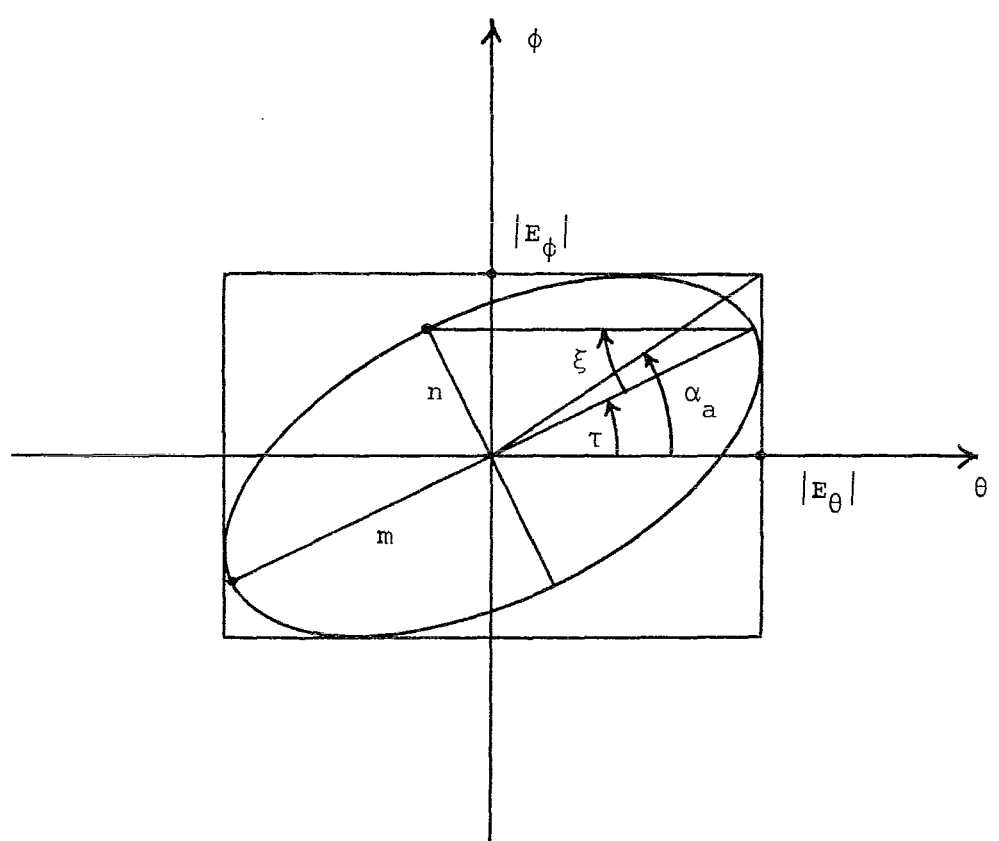


Figure D.1

APPENDIX E  
INTERMEDIATE MOMENT METHOD CODE CHECK VIA  
THE LOOP ANTENNA

The following figure shows the driving point admittance calculated by the Moment Method Computer code used to model the quadrifilar helical antennas discussed previously. The program and geometry was simplified by removing the radials and driving the loop at one point. The data was calculated using a loop radius to wire radius ratio of 500. The data is almost identical to that calculated by Harrington for the loop antenna [3].

